JOC Article

The *in, out* Asymmetric Pseudo-Triple Helical Form of a D_{3h} Diaza-Macropentacycle

Clément Bonnot,[†] Jean-Claude Chambron,*[,†] Enrique Espinosa,[†,‡] and Roland Graff[§]

Laboratoire d'Ingénierie Moléculaire pour la Reconnaissance et la Séparation des Métaux et des Molécules (ICMUB, UMR CNRS no 5260) Université de Bourgogne, 9 Avenue Alain Savary, 21078 Dijon, France, and Service Commun de RMN, Institut de Chimie (UMR CNRS no 7177), Université Louis Pasteur, 1 Rue Blaise Pascal, 67000 Strasbourg, France

jean-claude.chambron@u-bourgogne.fr

Received September 12, 2007

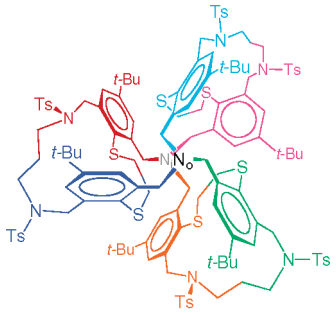

in, out (*io*) **5**

A sterically encumbered [N_2S_6] macropentacycle (**5**) related to diazamacrobicycles and cryptands has been synthesized in 53% yield by the [1+1] condensation reaction between functionalized macrocyclic and macrotricyclic precursors. A macrononacycle (**18**) resulting from the corresponding [2+2] condensation was isolated in 7% yield from the reaction mixture. Both compounds showed broad features in their room-temperature ^{1}H NMR spectra, but their maximal average symmetry (D_{3h} and D_{2h}, respectively) was achieved at high temperature (380 K). At low temperature (200 K, CD_2Cl_2 solution), the macropentacycle is "frozen" to a single asymmetric (C_1) conformation on the ^{1}H NMR time scale, which has also the molecular structure observed in the solid state by X-ray crystallography: pseudo-triple helical ($\neq C_3$) shape, *io* (*in*, *out*) form resulting from the endo/exo configuration at the nitrogen bridgehead atoms, and similar orientations of the tosyl substituents. The solution dynamics of the molecule can be described by coupled bridgehead nitrogen inversion, triple helix symmetrization, and reversal of triple helix handedness, with $\Delta G_c^{\ddagger} = 54.2$ kJ mol^{-1} in CD_2Cl_2 at 300 K. Adoption of the *io* form by macropentacycle **5** in the crystal and in solution at low-temperature most probably results from the steric crowding and strain introduced by the [15]ane-N_2S_2 macrocyclic bridging subunits.

Introduction

Macrobicyclic diamines are hollow molecules that can exist in three different forms, depending on the orientation of the lone pairs of the bridgehead nitrogen atoms with respect to the central cavity. As shown schematically in Figure 1, these forms are the symmetrical (*in*, *in*) (*ii*) for inside and (*out*, *out*) (*oo*) for outside orientation of the lone pairs, and the degenerate unsymmetrical (*in*, *out*) (*io*), for opposite orientations of the lone pairs. They represent the so-called homeomorphic isomers.[1,2]

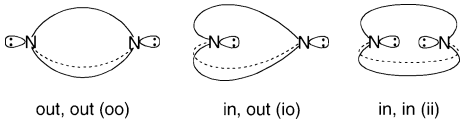

FIGURE 1. Homeomorphic isomers of diazamacrobicycles.

[†] Université de Bourgogne.
[‡] Current address: Laboratoire de Cristallographie et Modélisation des Matériaux Minéraux et Biologiques (LCM3B, UMR CNRS no 7036), Université Henri Poincaré-Nancy 1, boulevard des Aiguillettes, 54506 Vandoeuvre-lès-Nancy, France.
[§] Université Louis Pasteur.

10.1021/jo701984z CCC: $40.75
Published on Web 12/29/2007

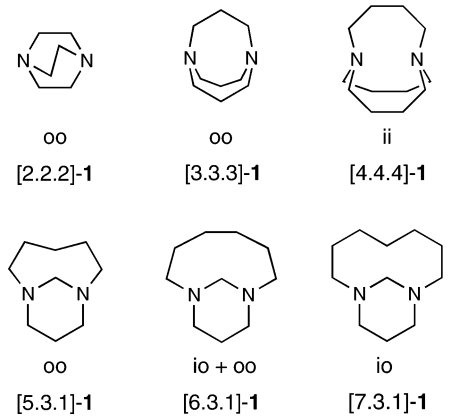

FIGURE 2. Preferred forms of small ring 1,(*k*+2)-diazabicyclo[*k.l.m*]-alkanes.

The prototypical macrobicyclic diamines are the 1,(*k*+2)-diazabicyclo[*k.l.m*]alkanes [*k.l.m*]-**1**, with selected examples shown in Figure 2.[2] With the exception of [2.2.2]-**1** (DABCO) and [3.3.3]-**1** (the *oo* form of the latter has flattened bridgehead nitrogens), symmetrical systems ($k = l = m \geq 4$) usually exist in the *ii* form, which minimizes interchain nonbonded interactions.[1,2] A transition from the symmetrical *oo* to the unsymmetrical *io* form was found in the series of unsymmetrical tetrahydropyrimidine derivatives [*k*.3.1]-**1**, for which the frontier lies at $k = 6$: [5.3.1]-**1** and [7.3.1]-**1** exist exclusively under the *oo* and *io* forms, respectively, no matter if they are in the gas phase or in solution, whereas [6.3.1]-**1** is a mixture of both, the *oo* form being favored in solution by comparison with the gas phase, because hydrogen bonding with the solvent ($CDCl_3$) stabilizes the more accessible exo sites.[3]

Other classical macrobicyclic diamines are the original cryptands [*k.l.m*]-**2**, where *k*, *l*, and *m* are the number of oxygen atoms in the chains (Figure 3).[4] The smallest member of the series [1.1.1]-**2** as well as its next higher symmetrical homologue [2.2.2]-**2** strongly favor the *ii* form, as shown by protonation studies,[5] molecular mechanics[6] and dynamics[7] calculations, and X-ray diffraction.[8] However, the latter molecule is more flexible and shows facile *in*, *out* interconversion.[5b] Prismand **3**, which is an extended analogue of [4.4.4]-**1**, also exists in the *ii* form.[9] Replacing the triethylamine-derived bridgeheads of [2.2.2]-**2** by *o*-benzylamine produces cryptand **4a**, which was shown to exist mainly in the *oo* form.[10a]

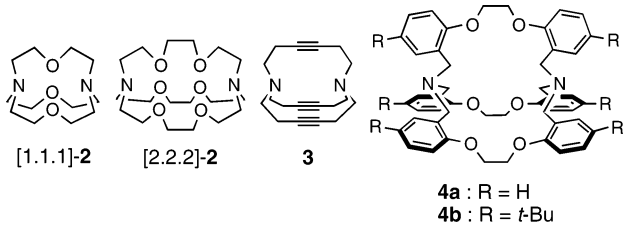

FIGURE 3. Examples of cryptands (**2**, **4**) and prismand **3**.

When not hindered, interconversions between the *ii*, *io* (*oi*), and *oo* forms proceed via nitrogen inversion[11] rather than homeomorphic isomerization.[2] The nitrogen inversion free energy barrier of [7.3.1]-**1** has been determined by variable temperature ^{13}C NMR spectroscopy: $\Delta G_{218}^{\ddagger} = 39.3$ kJ mol^{-1},[3] which is at the upper limit of the range observed for simple amines[12] but much lower than the values obtained for systems with CNC angle strain, such as aziridines[13] or 7-azanorbornanes[14] and related systems.[15] A similar value had been measured for larger [8.8.8]-**1** at 178 K,[1b] but the corresponding conformational change was later suggested to involve, rather than nitrogen inversion, torsional motions around single bonds of the bridges, as demonstrated for cryptands [1.1.1]-**2** ($\Delta G_{208}^{\ddagger} = 41$ kJ mol^{-1})[16] and [2.2.2]-**2** ($\Delta G_{148}^{\ddagger} = 27.2$ kJ mol^{-1})[4c] and prismand **3** ($\Delta G_{178}^{\ddagger} = 33.4$ kJ mol^{-1}).[9]

Macrobicycles showing the *in*, *out* isomerism are not limited to diamines. Systems containing N and C,[17] C-only,[18] and P-only[19] bridgeheads have been described. As the bridgehead atom cannot normally invert in the latter cases,[19c] when sterically possible, interconversion proceeds via homeomorphic isomer-

(1) (a) Park, C. H.; Simmons, H. E. *J. Am. Chem. Soc.* **1968**, *90*, 2428−2429. (b) Simmons, H. E.; Park, C. H.; Uyeda, R. T.; Habibi, M. F. *Trans. N. Y. Acad. Sci. Ser. II* **1970**, *32*, 521−534.

(2) Alder, R. W.; East, S. P. *Chem. Rev.* **1996**, *96*, 2097−2111.

(3) Alder, R. W.; Heilbronner, E.; Honegger, E.; McEwen, A. B.; Moss, R. E.; Olefirowicz, E.; Petillo, P. A.; Sessions, R. B.; Weisman, G. R.; White, J. M.; Yang, Z.-Z. *J. Am. Chem. Soc.* **1993**, *115*, 6580−6591.

(4) (a) Dietrich, B.; Lehn, J.-M.; Sauvage, J.-P. *Tetrahedron Lett.* **1969**, 2885−2888. (b) Cheney, J.; Lehn, J.-M.; Sauvage, J.-P.; Stubbs, M. E. *J. Chem. Soc., Chem. Commun.* **1972**, 1100−1101. (c) Dietrich, B.; Lehn, J.-M.; Sauvage, J.-P.; Blanzat, J. *Tetrahedron* **1973**, *29*, 1629−1645.

(5) (a) Pizer, R. *J. Am. Chem. Soc.* **1978**, *100*, 4239−4241. (b) Cox, B. G.; Schneider, H. *J. Chem. Soc., Perkin Trans 2* **1979**, 1293−1297. (c) Smith, P. B.; Dye, J. L.; Cheney, J.; Lehn, J.-M. *J. Am. Chem. Soc.* **1981**, *103*, 6044−6048.

(6) Geue, R.; Jacobson, S. H.; Pizer, R. *J. Am. Chem. Soc.* **1986**, *108*, 1150−1155.

(7) Troxler, L.; Wipff, G. *J. Am. Chem. Soc.* **1994**, *116*, 1468−1480.

(8) (a) Metz, B.; Moras, D.; Weiss, R. *J. Chem. Soc., Perkin Trans. 2* **1976**, 423−429. (b) Brügge, H.-J.; Carboo, D.; von Deuten, K.; Knöchel, A.; Kopf, J.; Dreissig, W. *J. Am. Chem. Soc.* **1986**, *108*, 107−112.

(9) Kunze, A.; Balalaie, S.; Gleiter, R.; Rominger, F. *Eur. J. Org. Chem.* **2006**, 2942−2955, and references cited therein.

(10) (a) Atkinson, I. M.; Lindoy, L. F.; Matthews, O. A.; Meehan, G. V.; Sobolev, A. N.; White, A. H. *Aust. J. Chem.* **1994**, *47*, 1155−1162. (b) Atkinson, I. M.; Carroll, A. R.; Janssen, R. J. A.; Lindoy, L. F.; Matthews, O. A.; Meehan, G. V. *J. Chem. Soc., Perkin Trans. 1* **1997**, 295−301. (c) Adam, K. R.; Atkinson, I. M.; Kim, J.; Lindoy, L. F.; Matthews, O. A.; Meehan, G. V.; Raciti, F.; Skelton, B. W.; Svenstrup, N.; White, A. H. *J. Chem. Soc., Dalton Trans.* **2001**, 2388−2397.

(11) (a) Lehn, J.-M. *Fortschr. Chem. Forsch.* **1970**, *15*, 311−377. (b) Lambert, J.-B. *Top. Stereochem.* **1971**, *6*, 19−105, and references cited therein.

(12) (a) Bushweller, C. H.; O'Neil, J. W. *J. Am. Chem. Soc.* **1970**, *92*, 2159−2160. (b) Dewar, M. J. S.; Jennings, W. B. *J. Am. Chem. Soc.* **1971**, *93*, 401−403. (c) Brown, J. H.; Bushweller, C. H. *J. Phys. Chem. A* **1997**, *101*, 5700−5706, and references therein.

(13) (a) Brois, S. J. *J. Am. Chem. Soc.* **1967**, *89*, 4242−4243. (b) Jautelat, M.; Roberts, J. D. *J. Am. Chem. Soc.* **1969**, *91*, 642−645. (c) Drakenberg, T.; Lehn, J.-M. *J. Chem. Soc., Perkin Trans 2* **1972**, 532−535.

(14) (a) Nelsen, S. F.; Ippoliti, J. T.; Frigo, T. B.; Petillo, P. A. *J. Am. Chem. Soc.* **1989**, *111*, 1776−1781. (b) Forsyth, D. A.; Zhang, W.; Hanley, J. A. *J. Org. Chem.* **1996**, *61*, 1284−1289. (c) Belostotskii, A. M.; Gottlieb, H. E.; Shokhen, M. *J. Org. Chem.* **2002**, *67*, 9257−9266, and references cited therein.

(15) (a) Malpass, J. R.; Tweddle, N. J. *J. Chem. Soc., Perkin Trans. 2* **1978**, 120−127. (b) Bushweller, C. H.; Brown, J. H.; Harpp, K. S.; Hirth, B. H.; Barden, T. C.; D'Albis, J. N.; Gribble, G. W. *J. Org. Chem.* **1998**, *63*, 3775−3777, and references cited therein.

(16) Cheney, J.; Kintzinger, J.-P.; Lehn, J.-M. *Nouv. J. Chim.* **1978**, *2*, 411−418.

(17) (a) Schrage, H.; Franke, J.; Vögtle, F.; Stekhan, E. *Angew. Chem., Int. Ed. Engl.* **1986**, *25*, 336−338. (b) Alajarín, M.; López-Lázaro, A.; Vidal, A.; Berná, J. *Chem.−Eur. J.* **1998**, *4*, 2558−2570.

(18) (a) Park, C. H.; Simmons, H. E. *J. Am. Chem. Soc.* **1972**, *94*, 7184−7186. (b) Haines, A. H.; Karntiang, P. *J. Chem. Soc., Perkin Trans. 1* **1979**, 2577−2587. (c) Franke, J.; Vögtle, F. *Angew. Chem., Int. Ed. Engl.* **1985**, *24*, 219−221.

(19) (a) Mitjaville, J.; Caminade, A.-M.; Majoral, J.-P. *J. Chem. Soc., Chem. Commun.* **1994**, 2161−2162. (b) Bauer, I.; Fröhlich, R.; Ziganshina, A. Y.; Prosvirkin, A. V.; Gruner, M.; Kazakova, E. K.; Habicher, W. D. *Chem.−Eur. J.* **2002**, *8*, 5622−5629, and references cited therein. (c) Exceptions have been reported: Alder, R. W.; Read, D. *Angew. Chem., Int. Ed.* **2000**, *39*, 2879−2882.

ization, which can be described as "the passage of any one chain through the ring formed by the other two chains and the bridgehead atoms".[20] Because the barrier to homeomorphic isomerization is usually higher than the barrier to nitrogen inversion, homeomorphic isomers could be separated by chromatography as, for example, in the case of *phosphorus*-based cryptands.[19b] *In*, *out* stereoisomerism has also been addressed in the case of cyclophanes.[21]

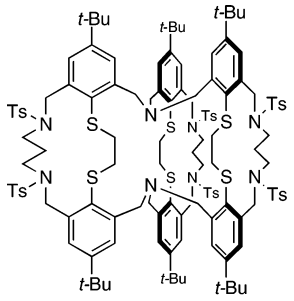

5

Diamine **5** derives from cryptand **4b**[10c] by substitution of the oxygen atoms of the latter with sulfur atoms and additional bridging of the benzyl groups with $-CH_2N(Ts)(CH_2)_3N(Ts)-CH_2-$ spacers that are anchored *ortho* to the S atoms. As a consequence, the linear bridges of macrobicyclic diamine **4b** are replaced by [15]ane-N_2S_2 macrocyclic bridges in **5**, which makes this system a macropentacyclic diamine. Its unique dynamic and protonation properties in the context of *in*, *out* isomerism and chirality have been already communicated.[22] This work examines in more detail the stereochemical properties of **5**. It shows that the macropentacycle adopts a unique pseudo-triple helical *io* form in solution at 200 K and in the solid state, achieving its maximal symmetry (D_{3h}) at 380 K, by a combination of three coupled processes: triple helix symmetrization, nitrogen inversion, and reversal of triple helicity.

Results and Discussion

Synthesis of the Macrocycles and Macropolycycles. Macrobicycles are usually synthesized as shown in Scheme 1a, by covalent bridging of a macrocycle (B),[4,10] a common alternative to the tripod capping route.[23] The corresponding [2+2] condensation reaction, whenever possible, leads to a macrotricycle (D).[4b,16] If, however, all three linear fragments incorporate a macrocyclic subunit each (Scheme 1b), then a macropentacycle (E) will be obtained, the [2+2] condensation product being in this case a macrononacycle (F). Such a macropentacyclic *intrinsic* topology has been previously obtained via either route.[24] Kyuphane, which derives from the cubic graph, and

SCHEME 1. Strategies for the Construction of Macrobicycles and Higher Order Macropolycycles

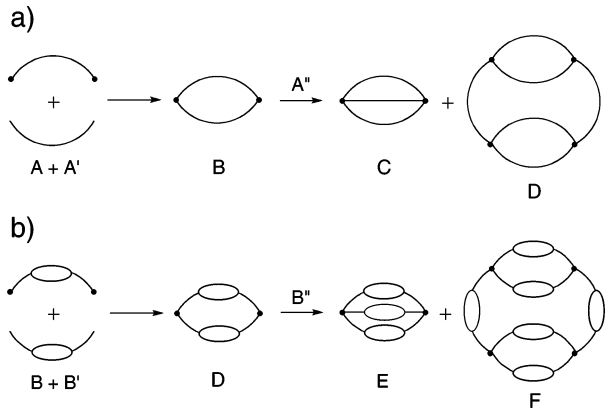

(a) Condensation of two functionalized linear fragments A and A′ leads to macrocycle B, which is further reacted with a third linear fragment (A″) to give macrobicycle C (and macrotricycle D). (b) The linear fragments of (a) are replaced by functionalized macrocycles (B, B′, and B″) to form successively macrotricycle D, macropentacycle E, and macrononacycle F.

the cylindrical macropentacycle are other exemples of macropentacyclic topologies.[25]

Nevertheless, the strategy presented above is reminiscent of the divergent construction of dendrimers, which involves the iterative duplication of atomic patterns.[26] Clearly, as in the case of dendrimers, the dimensionality of the macropolycycles obtained by this dichotomy process is limited for steric reasons.

The sequence of reactions leading to the three macrocyclic intermediates **10**, **14**, and **16** (respectively B, B′, B″ of Scheme 1b), and macrotricycle **17** (D of Scheme 1b), together with other potential precursors (**9**, **11**, and **15**) are detailed in Scheme 2.

The key starting material is tetraaldehyde **6**, previously developed by Kersting and co-workers as an organic template for making thiophenol-incorporating macrocycles in one-pot reactions.[27] In our synthetic scheme it was necessary to differentiate the two functions *ortho* to the sulfur, so that one would be connected to a bridgehead nitrogen, the other being included in the peripheral part of the [15]ane-N_2S_2 macrocyclic subunits of **5**. Reduction of tetraaldehyde **6** (1 equiv) with $NaBH_4$ (0.5 equiv) in THF/EtOH at 0 °C afforded diol **7** in 50% yield after chromatography, twice as much as the statistical yield (25%). Remarkably, the formation of the isomeric diol was not observed. The regioselectivity of the double reduction reaction could result from the decreased reactivity of the aldehyde meta to a benzylic alcohol function. An alternative is the intramolecular reduction of the second aldehyde function by the bound trihydroborate. For steric reasons, this may happen only when the aldehyde functions belong to two different aryl systems. In the next step, diol **7** was converted into electrophiles: reaction with $SOBr_2$ in the presence of pyridine in dichloromethane afforded the dibromo derivative **8** in 67% yield. Alternatively, the corresponding dichloride (**9**) was obtained in 73% yield by use of $SOCl_2$.

(20) Gregory, B. J.; Haines, A. H.; Karntiang, P. *J. Chem. Soc., Chem. Commun.* **1977**, 918−919.

(21) (a) Hohner, G.; Vögtle, F. *Chem. Ber.* **1977**, *110*, 3052−3077. (b) Nakazaki, M.; Yamamoto, K.; Toya, T. *J. Org. Chem.* **1981**, *46*, 1611−1615. (c) Dell, S.; Ho, D. M.; Pascal, R. A., Jr. *J. Org. Chem.* **1999**, *64*, 5626−5633.

(22) Bonnot, C.; Chambron, J.-C.; Espinosa, E. *J. Am. Chem. Soc.* **2004**, *126*, 11412−11413.

(23) (a) This discussion excludes transition metal template effects. (b) MacDowell, D.; Nelson, J. *Tetrahedron Lett.* **1988**, *29*, 385−386. (c) Beer, P. D.; Kocian, O.; Mortimer, R. J.; Spencer, P. *J. Chem. Soc., Chem. Commun.* **1992**, 602−604.

(24) (a) Wester, N.; Vögtle, F. *Chem. Ber.* **1980**, *113*, 1487−1493. (b) Wallon, A.; Werner, U.; Müller, W. M.; Nieger, M.; Vögtle, F. *Chem. Ber.* **1990**, *123*, 859−867.

(25) (a) Behr, J.-P.; Bergdoll, M.; Chevrier, B.; Dumas, P.; Lehn, J.-M.; Moras, D. *Tetrahedron Lett.* **1987**, *28*, 1989−1992. (b) Murakami, Y.; Kikuchi, J.-i.; Ohno, T.; Hirayama, T.; Hisaeda, Y.; Nishimura, H.; Snyder, J. P.; Steliou, K. *J. Am. Chem. Soc.* **1991**, *113*, 8229−8242.

(26) Tomalia, D. A.; Naylor, A. M.; Goddard, W. A., III. *Angew. Chem., Int. Ed. Engl.* **1990**, *29*, 138−175.

(27) (a) Kersting, B.; Steinfeld, G.; Fritz, T.; Hausmann, J. *Eur. J. Inorg. Chem.* **1999**, 2167−2172. (b) Klingele, M. H.; Kersting, B. *Z. Naturforsch.* **2001**, *56b*, 437−439.

SCHEME 2

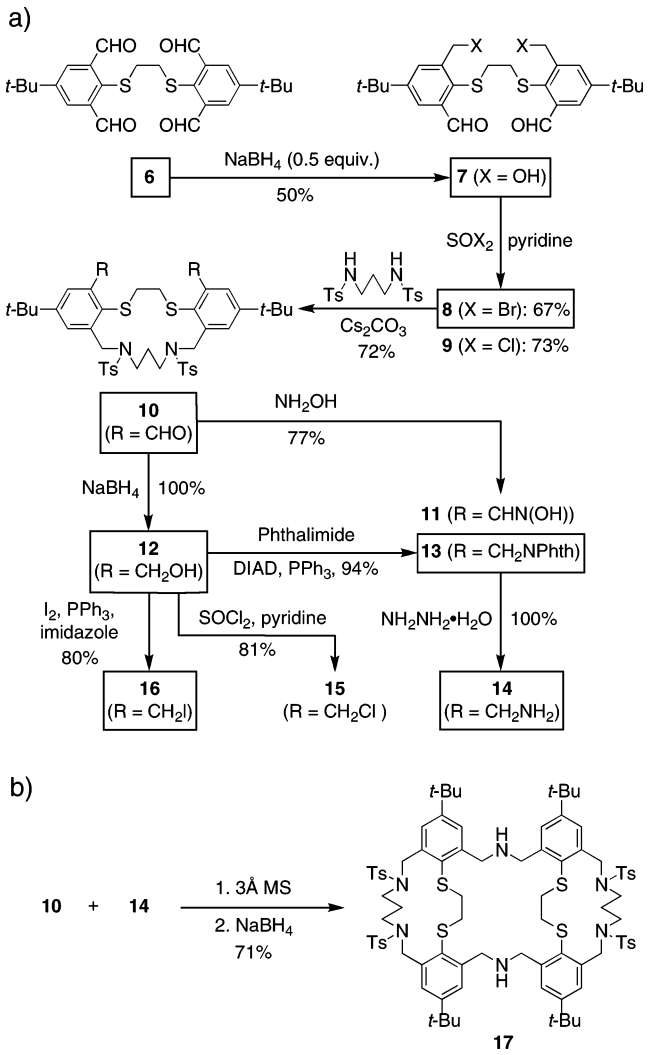

Construction of the first macrocycle (dialdehyde **10**) involved dibromo derivative **8** as the best electrophile. Reaction of **8** with *N*,*N*′-di-*p*-tosyl-1,3-diaminopropane in the presence of Cs_2CO_3 as base, in moderate dilution reaction conditions (13 mM in DMF, 35 °C), produced macrocyclic dialdehyde **10** in 72% yield. **10** represents an organic equivalent of the dialdehyde-functionalized Ni(II) complexes described as building blocks for unsymmetrical dithiophenolate-bridged complexes of compartmental ligands.[28] We planned to prepare the intermediate macrotricycle **17** by Schiff base condensation of dialdehyde **10** with the corresponding diamino derivative **14**, followed by $NaBH_4$ reduction. To this end, intermediate dioxime **11** was prepared by reaction of **10** with hydroxylamine in aqueous ethanol and isolated in 77% yield. However, our attempts to convert it to diamine **14** (catalytic hydrogenation or $LiAlH_4$) failed. Another route (Gabriel-type synthesis) was therefore developed. At first, dialdehyde **10** was reduced with $NaBH_4$ (MeOH, 0 °C) to macrocyclic diol **12**. The reaction was quantitative. Next, **12** was reacted with phthalimide in Mitsunobu reaction conditions (DIAD, PPh_3, THF, 0 °C)[29] to afford the diphthalimide derivative **13** in 94% yield after chromatographic purification. Hydrazinolysis in ethanol at reflux gave the desired diamino macrocycle **14** cleanly and quantitatively.

SCHEME 3

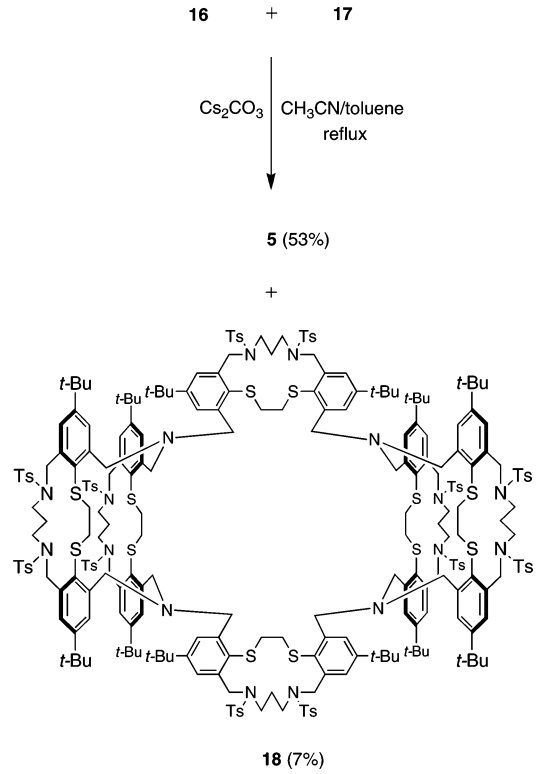

Two potentially useful electrophilic macrocycles were made from diol **12**: dichloro derivative **15** was obtained in 81% yield by reaction with $SOCl_2$/pyridine, whereas diiodo derivative **16** was isolated in 80% yield after reaction with I_2 in the presence of PPh_3 and imidazole (ratio 5:5:2) in dichloromethane at 0 °C.[30]

The next step in the construction of macropentacycle **5** involved at first Schiff base condensation of dialdehyde **10** with diamine **14** in the presence of 3 Å molecular sieves in diluted reaction medium (8 mM in CH_2Cl_2, 30 °C) followed by $NaBH_4$ reduction in MeOH/THF at 0 °C.[10c] Intermediate macrotricycle **17** was obtained in 71% yield after crystallization (Scheme 2b). The high yield observed for this macrocyclisation reaction can be rationalized in terms of preorganization of the reactants.[31] The reactive functions (aldehyde for **10**, amine for **14**) are placed pairwise on the same side of these 15-membered macrocycles, thus favoring the [1+1] cyclocondensation.

In the final step, macrotricycle **17** was reacted with macrocyclic diiodo derivative **16** in diluted medium (2.8 mM in 1:1 toluene/acetonitrile, 50 °C) and in the presence of Cs_2CO_3 as base (Scheme 3).[10c]

Macropentacycle **5** was best purified as its monoprotonated form (trifluoromethanesulfonate salt).[22] To this end, a controlled amount of trifluoromethanesulfonic acid was added to the reaction mixture after workup. Column chromatography of the crude allowed to isolate [**5**•H](CF_3SO_3) in 53% yield. Gratifyingly, macrononacycle **18** was obtained in 7% yield, albeit in

(28) Christensen, A.; Jensen, H. S.; McKee, V.; McKenzie, C. J.; Munch, M. *Inorg. Chem.* **1997**, *36*, 6080−6085.

(29) Mitsunobu, O. *Synthesis* **1981**, 1−28.

(30) (a) Garegg, P. J.; Samuelsson, B. *J. Chem. Soc., Chem. Commun.* **1979**, 978−980. See also: (b) Ireland, R. E.; Gleason, J. L.; Gegnas, L. D.; Highsmith, T. K. *J. Org. Chem.* **1996**, *61*, 6856−6872. (c) Merlic, C. A.; Aldrich, C. C.; Albaneze-Walker, J.; Saghatelian, A.; Mammen, J. *J. Org. Chem.* **2001**, *66*, 1297−1309.

(31) Cram, D. J. *Angew. Chem., Int. Ed. Engl.* **1986**, *25*, 1039−1057.

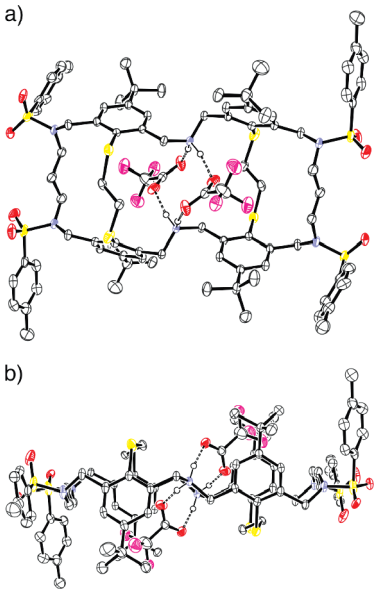

FIGURE 4. ORTEP views of diprotonated macrotricycle [**17**·2H](CF$_3$-CO$_2$)$_2$. (a) Top view. (b) Side view. The positions of hydrogen atoms shown here were refined. Other hydrogen atoms have been omitted for clarity. Thermal ellipsoids are drawn at 50% probability level.

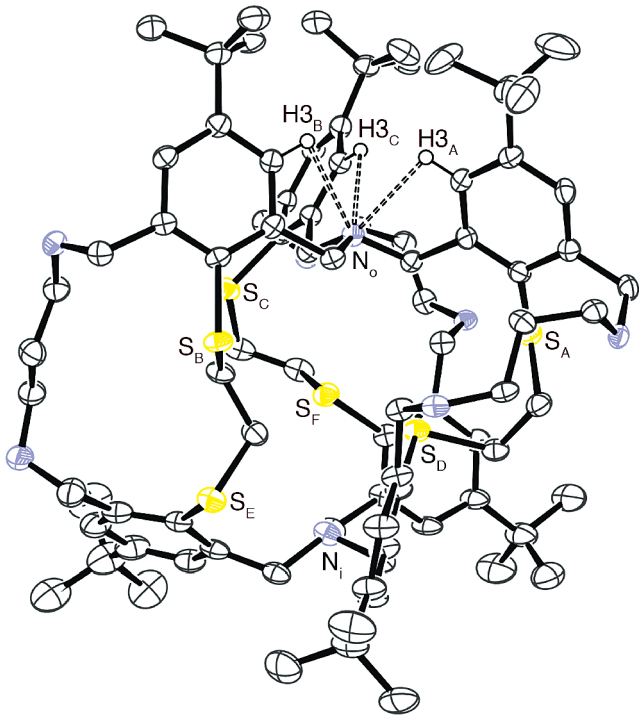

FIGURE 5. X-ray crystal structure of macropentacycle **5**: ORTEP side view. The tosyl groups and hydrogen atoms (H3$_A$, H3$_B$, and H3$_C$ excepted) have been omitted for clarity. Thermal ellipsoids are drawn at 50% probability level.

neutral form, in spite of the acidic treatment. The neutral form of macropentacycle **5** was recovered quasi quantitatively (98%) by reaction of [**5**·H](CF$_3$SO$_3$) with sodium methoxide. Preorganization of the reactants can again account for the relatively good yield of sterically crowded macropentacycle **5**. The formation of macrononacycle **18**,[32] which results from a [2+2] cyclocondensation reaction, is less favored entropically than that of **5**, which is the [1+1] cyclocondensation product. However, as shown by ^{1}H NMR (*vide infra*), **18** is apparently less strained and less sterically crowded than **5**. This favorable enthalpic factor may probably account for the observation and isolation of significant amounts of the macrononacycle in this reaction.

X-Ray Molecular Structure Analyses. All four macropolycycles reported in this work have been structurally characterized by single-crystal X-ray diffraction (Table S1, Supporting Information). Crystals of macrocycle **10**, a representative of the series of macromonocycles, were obtained from CH$_2$Cl$_2$/heptane. ORTEP views of the molecule are shown in Figure S1 (see Supporting Information). The aldehyde functions are obviously located on the same side of the molecule but, as the tosyl and supporting aryl groups, oriented in opposite directions with respect to the mean plane of the macrocycle.

Macrotricycle **17** could be crystallized from CH$_2$Cl$_2$/cyclohexane in its diprotonated form as the bis-trifluoroacetate salt, featuring a host−guest system in the solid state ([**17**·2H](CF$_3$-CO$_2$)$_2$). As shown in the ORTEP views of Figure 4, a crystallographic inversion center is located in the middle of the molecule. Each resulting half of the macrotricycle is cavity-shaped by the *t*-butylaryl (*t*-BuAr) walls. The bridgehead secondary amines are protonated, and the resulting ammoniums are hydrogen bound to the oxygen atoms of two trifluoroacetate anions that are sitting on top of the cavities, the CF$_3$ groups of the guests being sandwiched by the *t*-BuAr groups of the host. The distances *d*(H···O) are 1.71(1) and 1.73(1) Å, which, according to their relationship with dissociation energy *De* (eq 1):

$$De(\text{kJ mol}^{-1}) = 25\,000 \exp[-3.6d(\text{H}\cdots\text{O})]^{33} \qquad (1)$$

correspond to *De* values of 53 and 49 kJ mol^{-1} respectively. This is diagnostic of relatively strong hydrogen bonding interactions. In addition, all the C−O bond distances are identical to each other (1.237(4) Å), and the same is true for the N−H distances (1.02(1) Å), indicating that negative and positive charges are delocalized on carboxylate and ammonium groups, respectively.

The structure of macropentacycle **5** in protonated form has been discussed in an earlier report:[22] [**5**·H](CF$_3$SO$_3$) has a nearly perfect triple helical structure and takes up the *io* conformation in the solid state, the proton being localized on the endo bridgehead nitrogen atom N$_i$ and hydrogen-bound to the three proximal sulfur atoms. Crystals of **5** suitable for X-ray diffraction were obtained by deprotonation of acetonitrile solutions of [**5**·H](CF$_3$SO$_3$) with cryptand [2.2.2]-**2**. As shown in the ORTEP view of Figure 5, **5** has also the *io* conformation in the solid state. This result is quite surprising, because what was thought to be the driving force leading to the *io* conformation of [**5**·H]$^+$ (proton encapsulation in the N$_i$S$_3$ tetrahedral coordination sphere) is now lacking. However, as in the case of [**5**·H]$^+$, hydrogen bonding interactions (see also Figure S2a, Supporting Information) can be evidenced between the lone pair of the exo bridgehead nitrogen atom (N$_o$) and ortho (Ar)C-*H*′s, with H···N distances ranging from 2.46 (H3$_C$···N$_o$) and 2.48 (H3$_A$···N$_o$) to 2.64 Å (H3$_B$···N$_o$). Similar observations were

(32) The rare intrinsic macrononacyclic topology is also represented by a calix[4]arene/resorcarene conjugate. See: Timmerman, P.; Verboom, W.; van Veggel, F. C. J. M.; van Hoorn, W. P.; Reinhoudt, D. N. *Angew. Chem., Int. Ed. Engl.* **1994**, *33*, 1292−1295.

(33) Espinosa, E.; Molins, E.; Lecomte, C. *Chem. Phys. Lett.* **1998**, *285*, 170−173.

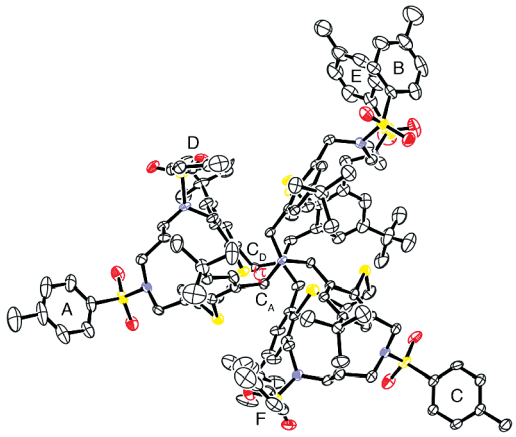

FIGURE 6. X-ray crystal structure of macropentacycle **5**: ORTEP top view from the exo bridgehead nitrogen atom. Hydrogen atoms have been omitted for clarity. Thermal ellipsoids are drawn at 50% probability level.

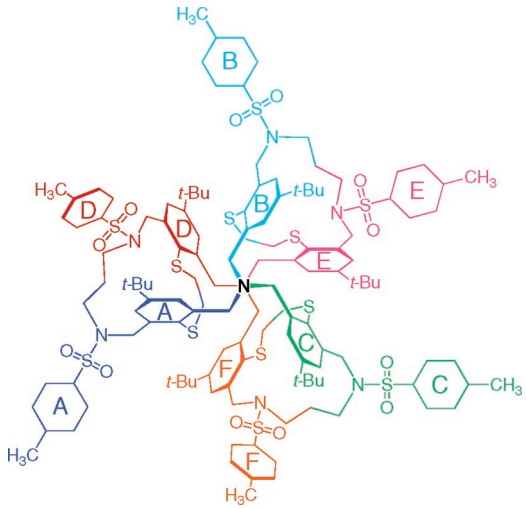

FIGURE 7. Schematic drawing of macropentacycle **5** (top view from the exo nitrogen) showing the 6 different sectors A, B, and C (exo side) and D, E, and F (endo side).

made by Lindoy and co-workers for the *oo* form of cryptand **4a**.[10a] Unlike [**5**·H]$^+$, which displays a very regular triple helical structure,[22] the triple helix of **5** in the crystal is not C_3-symmetric (Figure 6). It can be described as being made of the three branches AD, BE, and CF (made from the sectors A, B, C, D, E, and F) explicited in Figure 7 (see also Figure S10, Supporting Information). From Figures 5, 6, and 7, branch BE is clearly different from branches AD and CF, the latter being very similar to each other. The torsion angles τ that, for each branch of the molecule, correspond to the mean <C−N_i−N_o−C> value, range from 42.2 (branch AD, see Figure 6) and 45.5 (branch BE) to 49.9° (branch CF), the average value being 45.5°, which is lower than the value measured for [**5**·H](TfO) (49°).[22] This indicates that the molecule is less coiled in its neutral form. Accordingly, the distance between the bridgehead nitrogen atoms is longer than in the case of the proton adduct: 6.828 vs 6.325 Å. As shown in Figure S2b (see Supporting Information), unlike what is observed for [**5**·H]$^+$, the triangles (S_A, S_B, S_C) and (S_D, S_E, S_F) are not equilateral, pointing to a structure that is not as regular as in the case of the monoprotonated macropentacycle.

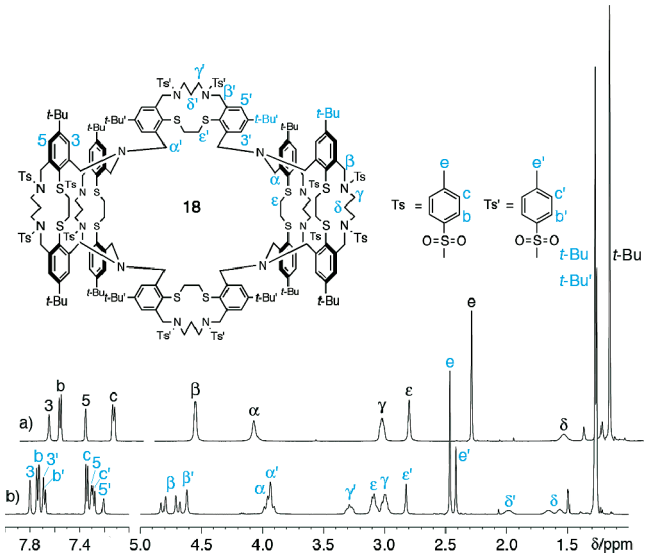

FIGURE 8. Comparison of the ^{1}H NMR spectra of (a) macropentacycle **5** and (b) macrononacycle **18** at 380 K (500 MHz, $C_2D_2Cl_4$).

Surprisingly, macrononacycle **18** crystallized in neutral form (from CH_2Cl_2/EtOAc), in spite of its acidic treatment (CF_3SO_3H) prior to SiO_2 chromatography and crystallization. A preliminary determination of its X-ray crystal structure is presented in Figure S3 (ORTEP view, see Supporting Information). The macrononacycle features two hinge-shaped cavities made from macrotricyclic subunits that are interconnected by two macrocyclic bridges and that host ethylacetate solvent molecules. All the tertiary amine bridgehead nitrogens have the exo configuration.

Solution Structure and Dynamics. Macrocycle **10**, macrotricycle **17**, macropentacycle **5**, and macrononacycle **18** are all constructed from the same [15]ane-N_2S_2 macrocyclic motif. In agreement with its symmetry properties (C_{2v}), macrotricycle **17** shows essentially the same ^{1}H NMR features as its precursor, plus the bridgehead α CH_2 protons, which appear at higher field than the β-CH_2. Whereas these species both show well-resolved signals at room temperature, this is not the case for the higher order macropenta- and macrononacycles **5** and **18**. In particular, the former (**5**) shows the broadest features in the series, which are indicative of the existence of slowly exchanging conformations on the NMR time scale (see below). The broadest spectra are obtained in $C_2D_2Cl_4$ and d^6-acetone (Figure S4, Supporting Information).

The dynamics of macropentacycle **5** in the 210−380 K temperature range have been investigated by VT NMR (Figures S5−S7, Supporting Information) in CD_2Cl_2 and $C_2D_2Cl_4$ solution. Stacked spectra recorded between 300 and 380 K are detailed in Figure S5 (see Supporting Information). A satisfactorily resolved spectrum of **5** over the full δ range is obtained at 380 K, where its maximum D_{3h} symmetry is achieved. This is due either to the presence of symmetrical *ii* and/or *oo* conformations and to the fast exchange of unsymmetrical *io* and *oi* conformations. Macrononacycle **18** shows broadened signals in the high-field region of the spectrum (1−4.6 ppm). Its maximal symmetry (D_{2h}) is again observed at 380 K (Figure S8, Supporting Information). Comparison of its 380 K spectrum with that of macropentacycle **5** (Figure 8) shows that all of its

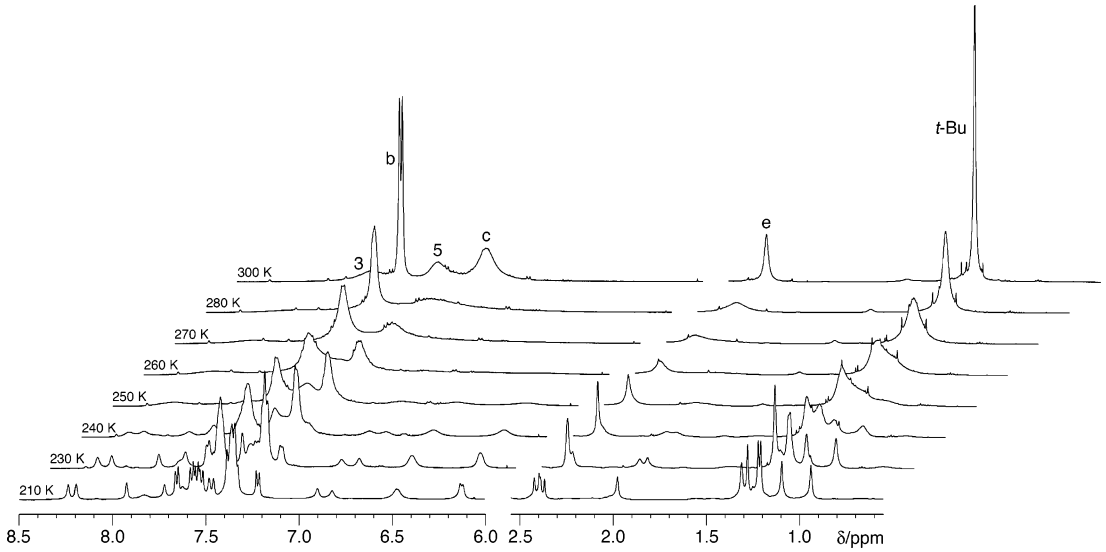

FIGURE 9. Stacked plot of the ^{1}H NMR spectra of macropentacycle **5** in the temperature range 210−300 K (500 MHz, CD_2Cl_2). The low field region is enhanced by a factor of 4.

signals are split in a 2:1 ratio. Indeed, the two bridging macrocycles are not equivalent to the four macrocycles of the macrotricyclic subunits. In addition, whereas the former contains one of the symmetry planes of the molecule and have enantiotopic methylene protons, this is not the case for the latter, the methylene protons of which are diastereotopic. This analysis is best illustrated by the δ, δ'-CH_2 and the β, β'-CH_2 protons. The δ, δ'-CH_2 protons show three signals between 1.5 and 2.0 ppm in a 1:1:1 ratio: a singlet for the enantiotopic δ'-CH_2 of the bridging macrocycles and two multiplets for the diastereotopic δ-CH_2 of the macrocyclic components of the macrotricyclic subunits. The β'-CH_2 protons of the bridging macrocycles appear as a singlet ($\delta = 4.615$ ppm), and the β-CH_2 of the macrotricyclic subunits display an AB pattern ($\delta = 4.75$ ppm; $J_{AB} = 17$ Hz, $\Delta\nu = 57$ Hz). The same is true for the bridgehead α, α'-CH_2; however, the singlet and the AB quartet are superposed at ca. 3.94 ppm.

Stacked spectra (8.5−6 and 2.5−0.5 ppm) of macropentacycle **5** in the low-temperature (300−210 K) range (CD_2Cl_2 solution) are shown in Figure 9 (the full δ range is displayed in Figure S7, Supporting Information). The 300 K spectrum recorded in CD_2Cl_2 is similar to the spectrum obtained at 320 K in $C_2D_2Cl_4$ (Figure S6, Supporting Information). At this temperature, the molecule still holds its D_{3h} symmetry, because the same number of signals as in the 380 K spectrum are observed, most clearly in the aromatic region. Upon cooling down further, the two aryl (Ts excepted) signals disappear briefly and give rise below 270 K to several broad signals that are scattered between 6 and 8.5 ppm. Simultaneously, the e (CH_3 of Ts) and *t*-Bu signals broaden unsymmetrically with intensity decrease and separate into individual singlets, which sharpen as the temperature is further lowered.

At 210 K, six different singlets for the *t*-Bu groups can be clearly identified between 0.9 and 1.4 ppm, as well as two sets of signals for the methyl (e) substituents of the tosyl groups in the 1.9−2.5 ppm range: a broad singlet at 1.95 ppm, which is clearly resolved into 2 singlets at 230 K, and 4 singlets between 2.3 and 2.5 ppm. The remainder of the aliphatic region (2.5−5.5 ppm) shows a quasi-continuum of signals (Figure S7, Supporting Information). The aromatic region shows well-resolved peaks between 6.0 and 8.5 ppm, whose integrals are all commensurate (Figure S9, Supporting Information). Comparison of the integral values in the full δ range indicates that only a single species, rather than a mixture of conformers, is present in solution at low temperature, contrary to our previous interpretation.[22]

This contrasts with the *diprotonated* cryptand ([2.2.2]-**2**·2H)$^{2+}$, the three forms of which (i^+i^+, o^+o^+, and i^+o^+) could be clearly identified at low temperature.[34] The fully assigned 200 K spectrum of macropentacycle **5** is shown in Figure 11. Colored labels of the protons are marked on the separated ORTEP views of the three branches AD, BE, and CF incorporating the six sectors A, B, C, D, E, and F of the molecule (Figure 10; see also Figure S10, Supporting Information).[35] The low-temperature structure of macropentacycle **5** in solution has been studied and solved using two-dimensional NMR (^{1}H/^{1}H COSY, ^{1}H/^{1}H ROESY and ^{1}H/^{13}C HSQC). Selected views of the 2D maps are shown in Figures 12−14. Other enlargements and the full 2D maps are included in Figures S11−S19 (see Supporting Information). The ROESY correlations are shown graphically in Figure S20. The following section shows that the low-temperature structures of macropentacycle **5** in the solution and in the crystal are correlated to each other.

The ^{1}H/^{1}H ROESY map of Figure S17 is detailed in Figures 12 and 13. Figure 12 highlights all the correlations between the six *t*-Bu groups and the proximal aryl protons 3 and 5. In addition to these, intercomponent correlations between *t*-Bu and tosyl (c and e) protons can be evidenced, such as *t*-Bu_A/c_D (*t*-Bu_A/e_D) and *t*-Bu_C/c_F (*t*-Bu_C/e_F), which indicate that the tosyl (Ts) groups D and F have the axial orientations shown in Figure 10a and c, respectively. That Ts_D (respectively Ts_F) lies in the groove formed by branches AD and BE (respectively CF and AD) as illustrated in Figures 6 and 7 is further supported by the correlations *t*-Bu_B/(c_D, e_D)(respectively *t*-Bu_A/(c_F, e_F)). Other correlations resulting directly from the axial orientation of Ts_D and Ts_F are: c_D/3_B (Figure S17, Supporting Information),α'_B/b_D and α'_A/b_F, as shown in Figure 13. Whereas axial Ts_D and

(34) MacGillivray, L. R.; Atwood, J. L. *J. Org. Chem.* **1995**, *60*, 4972−4973.

(35) Each branch, as represented, features the shape of a blade. Primed protons are located in the concave region of the blade, whereas unprimed ones are located in its convex part, see Figure S10 (Supporting Information).

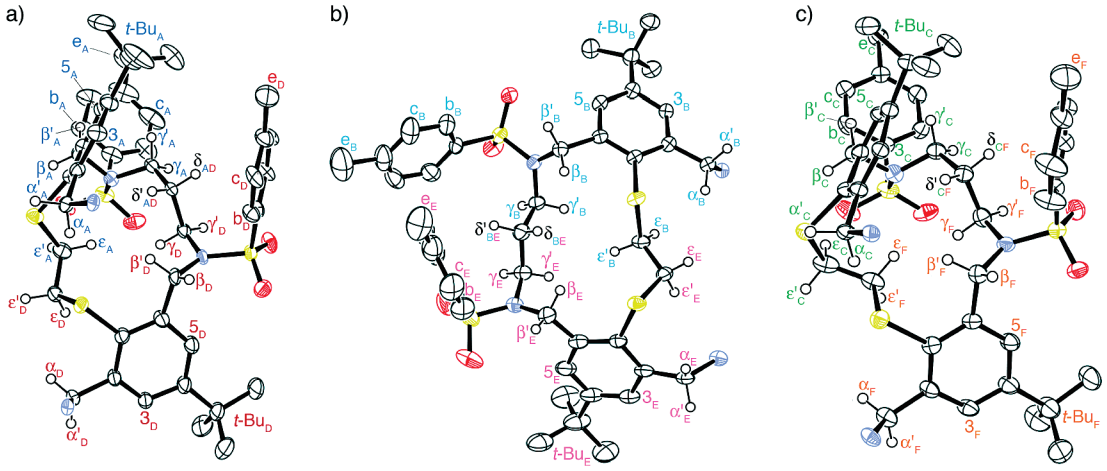

FIGURE 10. X-ray crystal structure of macropentacycle **5**. ORTEP views of the 3 isolated branches : (a) AD, (b) BE, and (c) CF with proton labels. Thermal ellipsoids are drawn at 50% probability level. Only methylenic hydrogen atoms are shown.

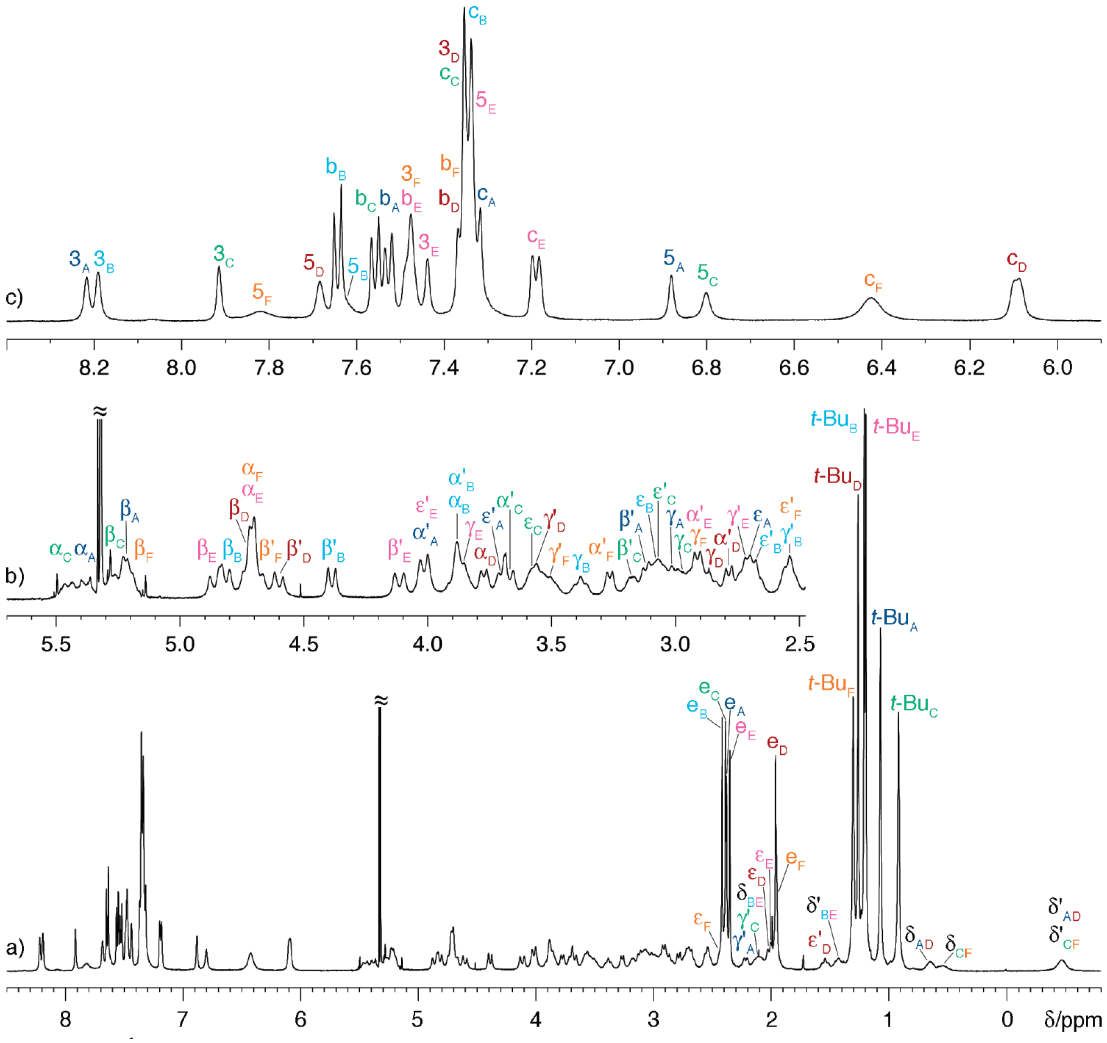

FIGURE 11. ^{1}H NMR spectrum of macropentacycle **5** at 200 K (500 MHz, CD_2Cl_2). (a) Full spectrum, (b) detail of the aliphatic region, and (c) detail of the aromatic region.

Ts_F interact only with the proximal β and γ' (i.e., β_D/b_D, β_F/b_F, γ'_D/b_D, and γ'_F/b_F), and δ_{AD} and δ_{CF} protons (i.e., b_D/δ_{AD} and b_F/δ_{CF}, Figure S18, Supporting Information), their analogues Ts_A and Ts_C correlate with β, β', and γ proximal protons (i.e., $(\beta_A, \beta'_A)/b_A$, $(\beta_C, \beta'_C)/b_C$, γ_A/b_A, and γ_C/b_C) because of their equatorial position (Figure 10a and c). Also for this reason, and contrary to axial Ts_D and Ts_F, they do not interact with other branches. Expectedly, aryl protons 5_A and 5_C interact with the nearby oriented β' and γ' protons (i.e., $\beta'_A/5_A$, $\gamma'_A/5_A$, $\beta'_C/5_C$, and $\gamma'_C/5_C$, Figures 13 and S17, Supporting Information). In

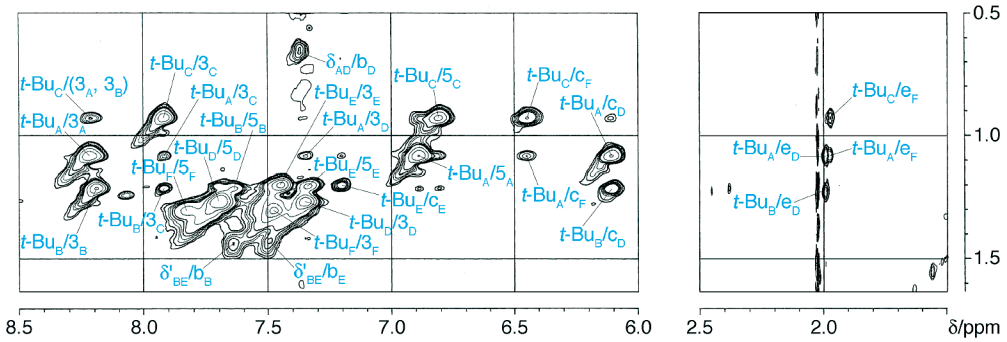

FIGURE 12. Detail of the NMR ^{1}H/^{1}H ROESY map of macropentacycle **5** at 200 K (500 MHz, CD_2Cl_2; mixing time: 450 ms).

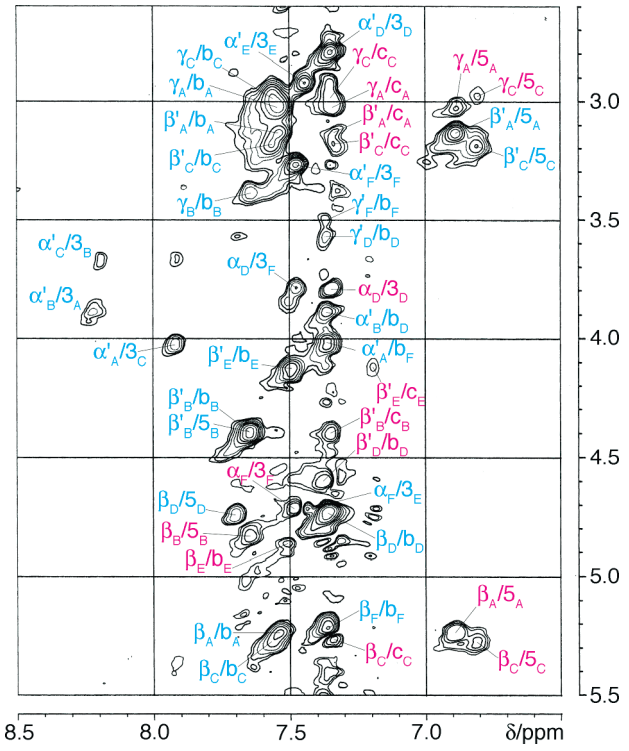

FIGURE 13. Detail of the NMR ^{1}H/^{1}H ROESY map of macropentacycle **5** at 200 K (500 MHz, CD_2Cl_2; mixing time: 450 ms). Spots corresponding to site exchange are labeled in magenta.

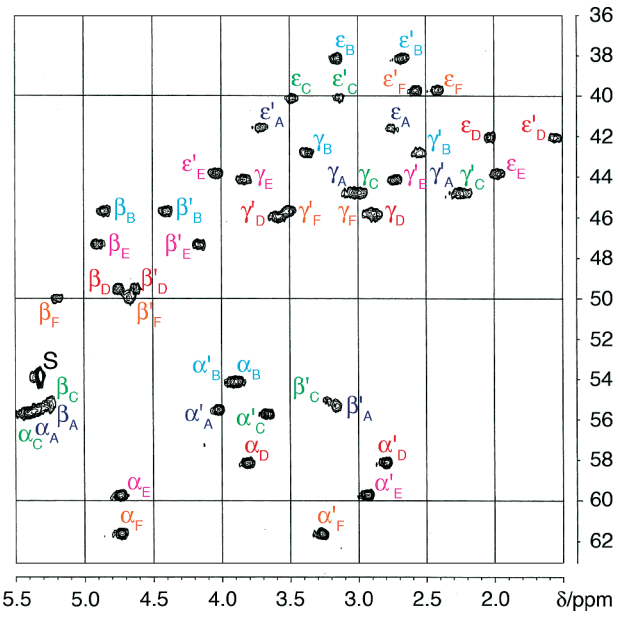

FIGURE 14. Detail of the NMR ^{1}H/^{13}C HSQC map of macropentacycle **5** at 219 K (500 MHz, CD_2Cl_2).

contrast to those involving Ts_A, Ts_C, Ts_D, and Ts_F, there are few correlations involving Ts_B and Ts_E (i.e., γ_B/b_B, δ'_{BE}/b_B, δ'_{BE}/b_E, β'_B/b_B, β'_E/b_E, and *t*-Bu_E/c_E), and none of them involves interbranch interactions, which agrees with the obvious peripheral orientation shown in Figure 10b.

Bridgehead methylenic α, α′ protons are clearly separated in two sets, which suggests that the molecule has the *io* form, with exo (A, B, C) and endo (D, E, F) propellers. Equatorial α'_A, α'_B, and α'_C correlate with 3_C, 3_A, and 3_B of the neighboring branch respectively, as would be expected for twisted *exo*-$NCH_\alpha H_{\alpha'}$ subunits. Expectedly, the corresponding axial α_A, α_B, and α_C protons do not show any correlation. The correlation $3_A/3_C$ (Figure S17, Supporting Information) indicates that the supporting aryl subunits are only slightly bent, which favors CH···N hydrogen bonding interactions between 3-Ar protons and the exo bridgehead nitrogen atom, as evidenced in the X-ray crystal structure (see Figures 2 and S2a, Supporting Information). The endo bridgehead methylenic α'_D, α'_E, and α'_F are axial and correlate with 3_D, 3_E, and 3_F of the same branch, respectively, whereas equatorial α_D and α_F protons correlate with 3_F and 3_E, respectively (see Figure 13).

All of the aliphatic protons can be identified in the HSQC maps. Pairs of methylene protons (α, α′), (*β*, *β*′), (*γ*, *γ*′), and (*ϵ*, *ϵ*′) are shown in Figure 14, whereas Figure S12 (see Supporting Information) details all (*δ*, *δ*′) pairs, the six methyl (e) of tosyl groups, and the six *t*-Bu systems. The relatively few ^{1}H/^{1}H ROESY correlations between nongeminal methylene protons are highlighted in Figures S11 and S19 (see Supporting Information). These correlations (ϵ'_A/β_A, ϵ'_B/β_E, ϵ'_F/α_F, ϵ_D/α_D, α'_F/α'_E, δ_{BE}/β_E, δ_{BE}/β_B, δ'_{AD}/β'_D, and δ_{AD}/γ'_D) are all consistent with the structures that can be predicted from the ORTEP representations of Figure 10 and confirm the assignements discussed above.

The fully assigned 200 K ^{1}H NMR spectrum (Figure 11) deserves several comments. Methyl e_D and e_F of axial Ts groups resonate upfield by comparison with the others (e_A, e_B, e_C, and e_E), because they lie in the shielding fields of *t*-$BuAr_B$ and *t*-$BuAr_A$ (for e_D), and *t*-$BuAr_A$ and *t*-$BuAr_C$ (for e_F), respectively. The same is true for c_D and c_F (respectively b_D and b_F), as compared to c_A, c_B, c_C, and c_E (respectively b_A, b_B, b_C, and b_E). Reciprocally, *t*-Bu_A and *t*-Bu_C are in the shielding fields of Ts_D and Ts_F, respectively. 5_A (and 5_C) are probably shielded also by Ts_D (and Ts_F). The deshielding of 3_A, 3_B, and 3_C, by comparison with 3_D, 3_E, and 3_F could be due to intramolecular

TABLE 1. Selected Probe Proton Pairs, DNMR Data and Free Energy Barriers at the Coalescence Temperature

probe protons	$\Delta\nu$ (Hz)	$k_c = \pi\Delta\nu/\sqrt{2}$ (s^{-1})	T_c (K)[a]	$\Delta G_c^{\ddagger}$ (kJ mol^{-1})[b]
β_C/β'_C	1049	2331[c]	300 (320[d])	54.2 (57.9[d])
δ_{CF}/δ'_{CF}	504	1120	280	52.1
$(e_A,e_B,e_C,e_E)/(e_D,e_F)$	202	449	260 (282[d,e])	50.2 (54.7[d,e])
β_C/β_E	207	460	260	50.1

[a] See Figure S21 (Supporting Information). [b] Calculated using the following relationship:[38a] $\Delta G_c^{\ddagger}$ (kJ mol^{-1}) = $2.303RT_c(10.319 + \log T_c - \log k_c)$, $R = 8.314$ $JK^{-1}mol^{-1}$. [c] For this pair of coupled protons, $\Delta\nu$ should be replaced by $(\Delta\nu^2 + 6J^2)^{1/2}$ in the calculation of k_c.[38b] However, because $6J^2 \ll \Delta\nu^2$, the simplified formula holds. [d] Values obtained in $C_2D_2Cl_4$. [e] See ref 22.

hydrogen bonding of the former with the exo bridgehead nitrogen atom, a feature clearly apparent in the X-ray crystal structure (Figures 5 and S2a, Supporting Information). All of the geminal methylenes show individual, mostly doublet signals, which indicates that they form diastereotopic pairs of atoms. Typical examples are: (α_C, α'_C), (α_A, α'_A), (β_E, β'_E), (β_B, β'_B), and (α_D, α'_D). ϵ'_D and γ_B show clear triplet signals in agreement with their anti relationship with vicinal ϵ_A and δ_{BE}, respectively (Figure 10). The lack of COSY and ROESY correlations between α_B and α'_B is due to the fact that these protons are nearly degenerate, as is apparent from the HSQC spectrum, with $\Delta\nu \approx 0$ and $^2J_{AB} \approx 18$ Hz. These protons excepted, all of the other geminal (α, α') systems show a very large $\Delta\nu$, e.g., 889 Hz for (α_C, α'_C). As noted in earlier reports, this indicates that the shielded H is oriented anti to the lone pair, the other being gauche.[36] This explains the apparently abnormal upfield resonance of α'_E and α'_D of *endo*-$NCH_\alpha H_{\alpha'}$, because of their removal from any aromatic shielding field. However, exactly the opposite is observed for α_A and α_C, which, according to the views of Figure 10a and c, should be oriented anti to the lone pair. In fact, these *exo*-$NCH_\alpha H_{\alpha'}$ protons lie in the deshielding field of the neighboring *t*-$BuAr_{(A,C)}$, and counter ring current effects could come into interplay. The highest anisotropy is noted for the pairs of diastereotopic protons (β_A, β'_A) and (β_C, β'_C) for which $\Delta\nu \approx 1050$ Hz. Finally, (δ_{AD}, δ'_{AD}) and (δ_{CF}, δ'_{CF}) show the strongest high-field resonances, because they are in the cumulative shielding fields of *t*-Bu_AAr and Ts_D on the one hand, and of *t*-Bu_CAr and Ts_F on the other hand (Figure 10). Such shieldings being absent in the case of (δ_{BE}, δ'_{BE}), these latter protons resonate at lower field than their homologues of branches AD and CF.

Macropentacycle **5** is asymmetric, because one of its three constitutive branches (BE) differs from the others (AD and CF). Although the two latter branches are very similar in the crystal structure (Figures 10a and c), they have different NMR signatures, because they do not have matched environments. Given the correlations found between the NMR data and the X-ray crystal structure, the molecule also takes up the *io* form and a nonsymmetrical (C_1), pseudo-triple helical chiral shape in solution at low temperature.

The complete assignement of the low-temperature ^{1}H NMR spectrum of macropentacycle **5** allows one to analyze in more detail the sequences of variable-temperature ^{1}H NMR spectra between 210 and 380 K shown in Figures 9 and S5−S7 (see Supporting Information). The $C_1 \rightarrow D_{3h}$ conversion of macropentacycle **5** within this temperature range can be virtually decomposed into three dynamic exchange processes: C_3 helix symmetrization, which exchanges branches AD, BE, and CF; bridgehead nitrogen inversion, which exchanges the *ii*, *io*, and *oo* forms; and triple helix inversion, which exchanges the right- and left-handed helical conformations and corresponds to a racemization process. All three processes are fast on the ^{1}H NMR time scale at $T \geq 360$ K, the spectra being consistent with D_{3h} symmetry of the molecule (Figure S5, Supporting Information).

The three dynamic processes identified above exchange homologous protons that either are diastereotopic (helix inversion), or belong to the same propeller (A, B, C) or (D, E, F) (helix symmetrization), or belong to two different sectors of the same branch, that is A and D, B and E, or C and F (nitrogen inversion). Several coalescence phenomena can be noted as the temperature is increased from 210 to 380 K in the composite stacked plot of Figure S21 (see Supporting Information). However, separation of those due to helix symmetrization and nitrogen inversion is rather delicate, because homologous probe protons for these latter processes resonate in the same regions of the spectrum. As a matter of proof, the signals of protons β_C and β_E, which are exchanged by a combination of these two processes, show coalescence (260 K). The same is true for the two groups of methyl protons e_D and e_F on the one hand and e_A, e_B, e_C, and e_E on the other hand. Due to extensive broadening between 260 and 320 K, it is not possible to track the signals of homologous protons in this temperature range. However, very broad features between 3.8 and 5.2 ppm at 300 K[37] follow transient sharpening of the 5 ppm signal (at 280 K) and precede the development of the α and β singlets between 340 and 380 K. They could be reasonably attributed to the coalescence of pairs of diastereotopic protons such as β_C and β'_C, which show the highest $\Delta\nu$ (1049 Hz) at the slow exchange temperature limit (200 K). In addition, coalescence of diastereotopic δ_{CF} and δ'_{CF} ($\Delta\nu = 504$ Hz) clearly does not occur below 280 K, which can be reasonably set as the T_c for this pair, because a very broad signal ($\delta \approx 0.25$ ppm) corresponding to δ'_{AD} (and overlapping δ'_{CF}) is last seen at 270 K.

Free energies of activation at the coalescence ($\Delta G_c^{\ddagger}$) can be estimated from $\Delta\nu$ and the coalescence temperatures (T_c).[38] They are collected in Table 1 for the pairs of probe protons examined above. Remarkably, all of these values are related in a linear fashion with the coalescence temperatures, which indicates that a unique dynamic process combines triple helix symmetrization, bridgehead nitrogen inversion, and reversal of triple helix handedness in the $C_1 \rightarrow D_{3h}$ conversion of macropentacycle

(36) (a) Hamlow, H. P.; Okuda, S.; Nakagawa, N. *Tetrahedron Lett.* **1964**, 2553−2559. (b) Graf, E.; Kintzinger, J.-P.; Lehn, J.-M.; LeMoigne, J. *J. Am. Chem. Soc.* **1982**, *104*, 1672−1678, note 20. (c) Bell, T. W.; Choi, H.-J.; Harte, W. *J. Am. Chem. Soc.* **1986**, *108*, 7427−7428.

(37) The ^{1}H NMR spectrum of **5** at 300 K in CD_2Cl_2 is very similar to the one obtained in $C_2D_2Cl_4$ at 320 K (Figure S21, Supporting Information).

(38) (a) Calder, I. C.; Garratt, P. J. *J. Chem. Soc. B* **1967**, 660−662. (b) Kost, D.; Carlson, E. H.; Raban, M. *J. Chem. Soc., Chem. Commun.* **1971**, 656−657. (c) Fischer, P.; Fettig, A. *Magn. Reson. Chem.* **1997**, *35*, 839−844.

5.[38c,39] The coupled processes have a free energy barrier of 54.2 kJ mol^{-1} at 300 K in CD_2Cl_2 (57.9 kJ mol^{-1} at 300 K in $C_2D_2Cl_4$).

Discussion

Comparison of the $\Delta G_c^{\ddagger}$ data obtained for macropentacycle **5** with those of the literature for related compounds in the context of helix and nitrogen inversion is difficult, if not impossible, given the hybrid nature of these dynamic processes in **5**.

Low-temperature dynamics of the relatively strained D_3-symmetrical cryptand [1.1.1]-**2** were attributed to helix inversion, which occurred with $\Delta G_c^{\ddagger} = 41.0$ kJ mol^{-1} at $T_c = 208$ K.[16] By extrapolation to this temperature, a value of $\Delta G_{208}^{\ddagger} = 44.9$ kJ mol^{-1} can be calculated for the combined processes taking place in macropentacycle **5**.[39] The small difference would suggest that helix inversion is an easier process in the latter system.

Literature data on the barriers to pyramidal nitrogen inversion in macrobicycles containing bridgehead nitrogen atoms are scarce.[3] In the case of simple acyclic alkylamines, they lie in the 21−40 kJ mol^{-1} range.[11] For example, dibenzylmethylamine has $\Delta G_c^{\ddagger} = 25.1$ kJ mol^{-1} at 127 K.[12a] Usually, the measured barriers correspond to net nitrogen inversion and concomitant N−C bond rotation,[40] the overall process being inversion dominant when trigonal planar nitrogen is the highest energy point (transition state).[41] Incorporation of the nitrogen atom in a cyclic structure increases the nitrogen inversion barrier dramatically when the CNC angle of the cycle has a value small enough to generate angle strain in the trigonal planar transition state. This situation is found in three-membered ring cyclic amines,[11,13] such as *N*-methylaziridine ($\Delta G_c^{\ddagger} = 79.7$ kJ mol^{-1} at 390 K),[13c] and to a lesser extent in azabicyclic systems with a rigid bicyclic framework,[11,14] such as 7-methyl-7-azanorbornane, which has $\Delta G_c^{\ddagger} = 57.6$ kJ mol^{-1} at 298 K in $CDCl_3$.[14a] Fortunately, the latter value can be directly compared to $\Delta G_{300}^{\ddagger} = 54.2$ kJ mol^{-1} obtained for macropentacycle **5**. This shows that, other intramolecular rearrangements contributing this free energy barrier, nitrogen inversion in macropentacycle **5** is probably a lower energy process, thus ranking this compound with ordinary alkylamines.

Conclusion

Transposition of a classical strategy for synthesizing cryptand-like macrobicycles has led to the efficient preparation (53%) of a sterically crowded [N_2S_6] macropentacycle (**5**) with nitrogen bridgehead atoms by [1+1] condensation reaction between a macrocycle and a macrotricycle. A macrononacycle (**18**), resulting from the corresponding [2+2] condensation, was obtained as byproduct in 7% yield. Both sterically crowded molecules show broad features in their room-temperature ^{1}H NMR spectra, which are indicative of slow motions on the NMR time scale. However, their maximal averaged symmetry (D_{3h} and D_{2h}, respectively) is achieved at high temperature (380 K). Cooling the temperature of a CD_2Cl_2 solution of the macropentacycle down to 200 K allows for the observation (at the NMR time scale) of a single species only, rather than a mixture of conformers. Remarkably, the structure of the low temperature conformer is asymmetric, yet the molecule holds a pseudo-triple helical shape, with endo and exo configurations of the bridgehead nitrogen atoms, as in the molecular structure obtained by single-crystal X-ray crystallography. The solution dynamics of the macropentacycle have been analyzed in terms of three processes: triple helix symmetrization, bridgehead nitrogen inversion, and reversal of triple helix handedness. All three of them are coupled with each other, $\Delta G_c^{\ddagger}$ being 54.2 kJ mol^{-1} in CD_2Cl_2 at 300 K. Macropentacycle **5** adopts the *io* C_1-symmetrical form not only in the solid state but also in solution at low temperature (at the NMR time scale). This latter feature is unique and shows that the *io* form, rather than simply resulting from intermolecular packing forces, has an intramolecular origin, which is most probably linked up with the steric crowding and strain introduced by the three [15]ane-N_2S_2 macrocyclic bridging subunits.

Experimental Section

General Information. All reactions were performed under argon using standard Schlenk techniques. Solvents were distilled over appropriate drying agents. All other chemicals were used as received.

X-Ray Crystallography. Colorless and prismatic single-crystal specimens of macrocycle **10**·0.25(CH_2Cl_2)·0.25(CH_3NHCH_3)·0.5(CH_3NHCHO), diprotonated macrotricycle [**17**·2H]·2CF_3CO_2·3(CH_2Cl_2), macropentacycle **5**·8.5(C_2H_3N), and macrononacycle **18** (from CH_2Cl_2/EtOAc) were selected for the X-ray diffraction experiments at $T = 115(2)$ K. Selected crystals were mounted with silicon grease on the tips of glass capillaries. Diffraction data were collected on a Nonius Kappa CCD diffractometer,[42] equipped with a nitrogen jet stream low-temperature system (Oxford Cryosystems). The X-ray source was graphite monochromatized Mo−Kα radiation ($\lambda = 0.71073$ Å) from a sealed tube. In all cases, lattice parameters were obtained by a least-squares fit to the optimized setting angles of the entire set of collected reflections. Intensity data were recorded as φ and ω scans with κ offsets. No significant intensity decay or temperature drift was observed during the data collections. Data reductions were done by using the DENZO software.[43] The structures were solved by direct methods using the SIR97 program.[44] Refinements were carried out by full-matrix least-squares on F^2 using the SHELXL97 program[45] and the complete set of reflections. Anisotropic thermal parameters were used for non-hydrogen atoms. The solvent molecules were found highly disordered in all the crystal structures, sometimes making the structure determinations very difficult. In spite of the fact that a first refinement of the molecular structure of macrononacycle **18** could be carried out (see Figure S3, Supporting Information), the too strong disorder of the solvent molecules could not permit one to clearly identify neither all the cocrystallised solvent molecules nor their number, leading to an incomplete crystal structure determination. In all cases, hydrogen

(39) The corresponding relationship is $y = 0.1009x + 23.9000$, $R^2 = 0.9992$.

(40) (a) Bushweller, C. H.; Anderson, W. G.; Stevenson, P. E.; Burkey, D. L.; O'Neil, J. W. *J. Am. Chem. Soc.* **1974**, *96*, 3892−3899. (b) Bushweller, C. H.; Anderson, W. G.; Stevenson, P. E.; O'Neil, J. W. *J. Am. Chem. Soc.* **1975**, *97*, 4338−4344. (c) Belostotskii, A. M.; Gottlieb, H. E.; Hassner, A. *J. Am. Chem. Soc.* **1996**, *118*, 7783−7789, and references cited therein.

(41) Anderson, J. E.; Tocher, D. A.; Casarini, D.; Lunazzi, L. *J. Org. Chem.* **1991**, *56*, 1731−1739.

(42) Nonius, B. In *COLLECT, Data Collection Software*; BV Nonius: Delft, The Netherlands, 1998.

(43) Otwinowski, Z.; Minor, W. *Methods Enzymol.* **1997**, *276*, 307−326.

(44) Altomare, A.; Burla, M. C.; Camalli, M.; Cascarano, G. L.; Giacovazzo, C.; Guagliardi, A.; Moliterni, A. G. G.; Polidori, G.; Spagna, R. *J. Appl. Crystallogr.* **1999**, *32*, 115−119.

(45) Sheldrick, G. M. In *SHELXS-97, Program for the Solution of Crystal Structures*; University of Göttingen: Göttingen, Germany, 1997.

atoms were fixed at calculated positions using a riding model, except those bonded to nitrogen atoms in the macrocycle and in the diprotonated macrotricycle, which were refined. A global isotropic thermal factor was refined for the hydrogen atoms of the crystal structures of **10** and [**17**·2H]. For **5**·8.5(C_2H_3N), their thermal factor was fixed to 1.5 times that of its bonded atom (i.e., for X−H : U(H) = 1.5 Ueq(X)). Crystallographic views were generated using ORTEP III for Windows.[46]

NMR Spectroscopy. Low-temperature 2D NMR experiments were performed at 500.13 (^{1}H) and 121.77 (^{13}C) MHz, using a Broad Band Inverse probe equipped with Z-gradients (BBI/GrZ). Relaxation delays were 3 s; 4K × 512 data matrices were processed in 4K × 2K (ROESY) and 4K × 4K (HSQC) sizes. HSQC spectra were obtained with inverse sequences and Z-gradients. ROESY spectra were obtained off resonance at a 54.7° angle, using adiabatic spin lock pulses, the mixing times ranging from 250 to 450 ms.[47]

1,2-Bis(4-*tert*-butyl-2-formyl-6-hydroxymethylphenylsulfanyl)-ethane 7. To a chilled solution of tetraaldehyde **6**[27] (3.579 g, 7.6 mmol) in THF (300 mL) and absolute ethanol (90 mL) was added sodium borohydride (0.145 g, 0.214 mmol). After 1 h of stirring at 0 °C, sodium hydrogencarbonate (5% aqueous solution, 90 mL) was added. The reaction mixture was diluted with water (250 mL) and extracted with dichloromethane (250 mL). The organic layer was dried ($MgSO_4$), filtered, and evaporated. Gradient column chromatography (silica, 1:1 dichloromethane/pentane, 0.5% methanol in dichloromethane gradient) afforded 1.790 g of **7** in 49.6% yield as a colorless solid, mp 148.5−150.5 °C; ^{1}H NMR (500 MHz, $CDCl_3$): δ 1.35 (s, 18H; *t*-Bu-*H*), 2.13 (br s, 2H; OH), 2.86 (s, 4H; ϵ-H), 4.89 (s, 4H; β-H), 7.78 (d, ^4J = 2.4 Hz, 2H; 5-H), 7.88 (d, ^4J = 2.4 Hz, 2H; 3-H), 10.68 ppm (s, 2H; C*H*O); ^{13}C NMR (75 MHz, $CDCl_3$): δ 31.3 (C(*C*H$_3$)$_3$), 35.3 (*C*(CH$_3$)$_3$), 38.0 (ϵ-C), 63.5 (β-C), 125.7 (3-C), 131.8 (5-C), 132.8 (1-C), 138.0 (2-C), 145.9 (6-C), 153.5 (4-C), 193.3 ppm (*C*HO); IR (neat): ν 1046 (s, CH$_2$−O), 1685 (vs, CO), 2868 and 2962 (s, C(O)-H), 3377 cm^{-1} (m, br, OH); elemental analysis calcd (%) for $C_{26}H_{34}O_4S_2$·0.5CH_3OH (490.71): C 64.86, H 7.39, S 13.07; found: C 64.95, H 7.44, S 13.06.

1,2-Bis(4-*tert*-butyl-2-formyl-6-bromomethylphenylsulfanyl)-ethane 8. Thionyl bromide (0.10 mL, 0.71 mmol) was added to a solution of diol **7** (0.150 g, 0.31 mmol) and pyridine (0.05 mL, 0.62 mmol) in dichloromethane (4 mL) at 0 °C. After stirring for 4.5 h under gentle reflux, the reaction mixture was diluted with dichloromethane (40 mL) and washed with water (3 × 40 mL). The combined organic phases were dried ($MgSO_4$) and filtered, and the solvent was evaporated to dryness. Column chromatography (silica, 7:1 dichloromethane/pentane) of the crude product combined from two identical runs afforded 0.255 g (67% yield) of **8** as a brown solid, mp 144−147 °C; ^{1}H NMR (300 MHz, $CDCl_3$): δ 1.35 (s, 18H; *t*-Bu-*H*), 2.96 (s, 4H; ϵ-H), 4.82 (s, 4H; β-H), 7.73 (d, ^4J = 2.4 Hz, 2H; 5-H), 7.90 (d, ^4J = 2.4 Hz, 2H; 3-H), 10.67 ppm (s, 2H; C*H*O); ^{13}C NMR (75 MHz, $CDCl_3$): δ 31.3 (C(*C*H$_3$)$_3$), 31.8 (β-C), 35.3 (*C*(CH$_3$)$_3$), 37.9 (ϵ-C), 126.9 (3-C), 133.9 (5-C), 134.1 (1-C), 138.6 (2-C), 143.5 (6-C), 153.8 (4-C), 192.9 ppm (*C*HO); IR (neat): ν 1681 (vs, CO), 2856 and 2955 (s, C(O)-H), 3068 cm^{-1} (w, ArH); HRMS (ESI): calcd for $C_{26}H_{32}Br_2NaO_2S_2$ [M + Na$^+$], 621.01027; found 621.00855.

1,2-Bis(4-*tert*-butyl-2-formyl-6-chloromethylphenylsulfanyl)-ethane 9. Thionyl chloride (0.10 mL, 1.3 mmol) was added to a solution of diol **7** (0.300 g, 0.63 mmol) and pyridine (0.11 mL, 1.3 mmol) in dichloromethane (8 mL) at 0 °C. After stirring for 2 h at 0 °C and 3 h at room temperature, the reaction mixture was diluted with dichloromethane (40 mL) and washed with water (2 × 40 mL). The water layer was extracted back with dichloromethane (2 × 20 mL). The combined organic phases were dried ($MgSO_4$), filtered, and evaporated to dryness. Column chromatography (silica, 1:1 dichloromethane/heptane) afforded 0.485 g (73% yield) of **9** as a pale-yellow solid, mp 139−140 °C; ^{1}H NMR (300 MHz, $CDCl_3$): δ 1.35 (s, 18H; *t*-Bu-*H*), 2.91 (s, 4H; ϵ-H), 4.90 (s, 4H; β-H), 7.74 (d, ^4J = 2.4 Hz, 2H; 5-H), 7.92 (d, ^4J = 2.4 Hz, 2H; 3-H), 10.69 ppm (s, 2H; C*H*O); ^{13}C NMR (75 MHz, $CDCl_3$): δ 31.3 (C(*C*H$_3$)$_3$), 35.4 (*C*(CH$_3$)$_3$), 38.0 (ϵ-C), 44.5 (β-C), 126.9 (3-C), 133.7 (5-C), 134.1 (1-C), 138.5 (2-C), 143.0 (6-C), 153.8 (4-C), 192.9 ppm (*C*HO); IR (neat): ν 1679 (vs, CO), 2867 and 2958 (s, C(O)-H), 3070 cm^{-1} (w, ArH); MS (70 eV, EI): *m*/*z* (%): 511 (9) [M$^+$].

Macrocycle 10. To a suspension of cesium carbonate (9.05 g, 27.8 mmol) in DMF (270 mL) at 35 °C was slowly added (80 min) a mixture of dibromide **8** (2.823 g, 4.70 mmol) and *N*,*N*′-di-*p*-tosyl-1,3-diaminopropane (2.1 g, 5.5 mmol) in DMF (90 mL). The reaction was further stirred for 30 min, and the solvent was removed in vacuo. The residue was taken up in dichloromethane (250 mL) and water (150 mL). The aqueous layer was extracted with dichloromethane (3 × 30 mL). The organic layer was finally washed with brine (3 × 50 mL), dried ($MgSO_4$), and filtered, and the solvent was evaporated. Column chromatography (silica, 1:1 dichloromethane/heptane, dichloromethane gradient) afforded 2.79 g (72% yield) of **10** as a pale-yellow solid, mp 193 °C; ^{1}H NMR (300 MHz, $CDCl_3$): δ 1.23 (s, 18H; *t*-Bu-*H*), 1.67 (br m, 2H; δ-H), 2.43 (s, 6H; C*H*$_3$), 2.92 (s, 4H; ϵ-H), 3.09 (t, ^3J = 7.7 Hz, 4H; γ-H), 4.61 (s, 4H; β-H), 7.31 (d, ^3J = 8.3 Hz, 4H; c-H), 7.61 (d, ^4J = 2.4 Hz, 2H; 5-H), 7.68 (d, ^3J = 8.3 Hz, 4H; b-H), 7.83 (d, ^4J = 2.4 Hz, 2H; 3-H), 10.60 ppm (s, 2H; C*H*O); ^{13}C NMR (75 MHz, $CDCl_3$): δ 21.9 (*C*H$_3$), 25.8 (δ-C), 31.1 (C(*C*H$_3$)$_3$), 35.2 (*C*(CH$_3$)$_3$), 39.4 (ϵ-H), 45.1 (γ-C), 48.4 (β-C), 126.5 (3-C), 127.4 (b-C), 130.3 (c-C), 132.0 (5-C), 133.1 (1-C), 137.3 (2-C), 137.7 (a-C), 141.2 (6-C), 144.0 (d-C), 153.5 (4-C), 192.7 ppm (*C*HO); IR (neat): ν 1688 (vs, CO), 2868 and 2960 cm^{-1} (s, C(O)-H); HRMS (ESI): calcd for $C_{43}H_{52}N_2NaO_6S_4$ [M + Na$^+$], 843.26004; found 843.25736.

Macrocycle 11. A solution of hydroxylamine·HCl (0.168 g, 2.41 mmol) in 5% aqueous sodium hydroxide (2.5 mL) was added to a solution of macrocycle **10** (0.200 g, 0.24 mmol) in absolute ethanol (5 mL). After 3 h reflux, the reaction mixture was diluted with dichloromethane (100 mL) and water (50 mL). The organic layer was washed with water (2 × 25 mL), dried ($MgSO_4$), and filtered, and the solvents were evaporated. Column chromatography (silica, dichloromethane, 5% methanol in dichloromethane gradient) afforded 0.160 g (77% yield) of **11** as a colorless solid, mp 255−256 °C; ^{1}H NMR (300 MHz, $CDCl_3$): δ 1.21 (s, 18H; C(C*H*$_3$)$_3$), 1.62 (br m, 2H; δ-H), 2.44 (s, 6H; C*H*$_3$), 2.78 (s, 4H; ϵ-H), 3.09 (t, ^3J = 7.7 Hz, 4H; γ-H), 4.56 (s, 4H; β-H), 7.32 (d, ^3J = 8.3 Hz, 4H; c-H), 7.40 (d, ^4J = 2.1 Hz, 2H; 5-H), 7.68 (d, ^4J = 2.1 Hz, 2H; 3-H), 7.69 (d, ^3J = 8.3 Hz, 4H; b-H), 8.27 (br s, 2H, NOH), 8.70 ppm (s, 2H; α-H); ^{13}C NMR (75 MHz, $CDCl_3$): δ 21.7 (*C*H$_3$), 26.1 (δ-H), 31.1 (C(*C*H$_3$)$_3$), 34.9 (*C*(CH$_3$)$_3$), 37.7 (ϵ-C), 45.3 (γ-H), 49.2 (β-H), 123.9 (3-C), 127.3 (b-C), 127.8 (5-C), 129.1 (1-C), 130.1 (c-C), 135.6 (2-C), 137.1 (a-C), 140.3 (6-C), 143.7 (d-C), 150.2 (α-C), 152.8 ppm (4-C); IR (neat): ν 970 (s, N−OH), 2958 (m, NC−H), 3299 cm^{-1} (w, O−H); HRMS (ESI): calcd for $C_{43}H_{54}N_4NaO_6S_4$ [M + Na$^+$], 873.28184; found 873.28376.

Macrocycle 12. Sodium borohydride (0.14 g, 0.37 mmol) was added to a solution of dialdehyde **10** (0.500 g, 0.61 mmol) in methanol (80 mL) at 0 °C. After 1 h of stirring, sodium hydrogencarbonate (5% aqueous solution, 20 mL) was added to the reaction mixture, which was subsequently taken up in dichloromethane (200 mL) and water (100 mL). The organic layer was washed with water (2 × 100 mL), dried ($MgSO_4$), and filtered, and the solvents were evaporated, affording macrocycle **12** (0.500 g) quantitatively as a colorless solid, mp 180−184 °C; ^{1}H NMR (300 MHz, $CDCl_3$): δ 1.21 (s, 18H; C(C*H*$_3$)$_3$), 1.62 (br m, 2H; δ-H), 2.17 (t, ^3J = 6.1 Hz, 2H; OH), 2.43 (s, 6H; C*H*$_3$), 2.93 (s, 4H; ϵ-H), 3.03 (t, ^3J = 7.8 Hz, 4H; γ-H), 4.61 (s, 4H; β-H), 4.83 (d, ^3J = 6.1 Hz, 4H; α-H), 7.24 (d, ^4J = 2.4 Hz, 2H; 5-H), 7.30 (d, ^3J = 8.3 Hz, 4H; c-H), 7.38 (d, ^4J = 2.4 Hz, 2H; 3-H), 7.69 ppm

(46) Farrugia, L. J. *J. Appl. Crystallogr*. **1999**, *32*, 837−838.

(47) (a) Bax, A.; Davis, D. G. *J. Magn. Reson.* **1985**, *63*, 207−213. (b) Desvaux, H.; Berthault, P.; Birlirakis, N.; Goldman, M.; Piotto, M. *J. Magn. Reson. A* **1995**, *113*, 47−52.

(d, ^3J = 8.3 Hz, 4H; b-H); ^{13}C NMR (75 MHz, $CDCl_3$): δ 21.9 (CH_3), 26.1 (δ-C), 31.3 (C(CH_3)$_3$), 35.1 (C(CH$_3$)$_3$), 37.4 (ϵ-C), 45.0 (γ-C), 49.7 (β-C), 65.0 (α-C), 125.9 and 126.0 (3-C and 5-C), 127.5 (b-C), 127.8 (1-C), 130.3 (c-C), 137.5 (a-C), 140.6 (6-C), 143.8 (d-C), 145.1 (2-C), 153.4 ppm (4-C); HRMS (ESI): calcd for $C_{43}H_{56}N_2NaO_6S_4$ [M + Na^+], 847.29134; found 847.29411.

Macrocycle 13. DIAD (4.10 mL, 20.72 mmol) was slowly added to a solution of macrocycle **12** (5.7 g, 6.9 mmol), phthalimide (3.05 g, 20.72 mmol), and triphenylphosphine (5.44 g, 20.72 mmol) in THF (235 mL) at 0 °C. After stirring the reaction mixture for 3 h at 0 °C, the solvent was evaporated and the residue was dissolved in dichloromethane (300 mL). The organic layer was washed with 5% aqueous sodium hydroxide (3 × 150 mL). The aqueous layer was extracted back with dichloromethane (2 × 100 mL). The combined organic extracts were washed with water (3 × 250 mL) until neutrality, dried ($MgSO_4$), and filtered, and the solvent was evaporated. Column chromatography (silica, 20% heptane in dichloromethane, dichloromethane gradient) afforded a first crop of pure **13** (4.31 g). Further amounts (2.72 g) were obtained by crystallization from 1:2 dichloromethane/ethanol. Total yield : 94%. **13**, mp 171−173 °C; ^{1}H NMR (300 MHz, $CDCl_3$): δ 1.11 (s, 18H; C(CH_3)$_3$), 1.66 (br m, 2H; δ-H), 2.42 (s, 6H; CH_3), 3.06 (s, 4H; ϵ-H), 3.08 (t, ^3J = 8.1 Hz, 4H; γ-H), 4.67 (s, 4H; β-H), 5.21 (s, 4H; α-H), 7.15 (d, ^4J = 2.4 Hz, 2H; 3-H), 7.26 (d, ^4J = 2.4 Hz, 2H; 5-H), 7.30 (d, ^3J = 8.3 Hz, 4H; c-H), 7.70 (d, ^3J = 8.3 Hz, 4H; b-H), 7.74 (dd, ^3J = 3.2 Hz, ^4J = 5.6 Hz, 4H; δ'-H), 7.88 ppm (dd, ^3J = 3.2 Hz, ^4J = 5.6 Hz, 4H; γ'-H); ^{13}C NMR (75 MHz, $CDCl_3$): δ 21.9 (CH_3), 25.5 (δ-C), 31.2 (C(CH_3)$_3$), 35.0 (C(CH$_3$)$_3$), 37.0 (ϵ-C), 40.7 (α-C), 44.9 (γ-C), 49.5 (β-C), 123.8 (γ'-C), 124.6 (3-C), 125.3 (5-C), 127.5 (b-C), 127.7 (1-C), 130.3 (c-C), 132.4 (β'-C), 134.5 (δ'-C), 137.7 (a-C), 140.8 (6-C and 2-C), 143.7 (d-C), 153.1 (4-C), 168.6 ppm (α'-C); MS (LSI-MS): *m*/*z* (%): 1083 (100) [M^+], 927 (81) [M^+ − Ts]; elemental analysis calcd (%) for $C_{59}H_{62}N_4O_8S_4$ (1083.43): C 65.41, H 5.77, N 5.17; found: C 65.37, H 5.70, N 5.16.

Macrocycle 14. Hydrazine hydrate (3.15 mL, 64.8 mmol) was added to a suspension of macrocycle **13** (7.03 g, 6.48 mmol) in refluxing ethanol (800 mL). After 4 h of reaction, the solvent was evaporated and the residue was taken up in dichloromethane (600 mL). The organic layer was washed with 5% aqueous sodium hydroxide (2 × 250 mL) and then water (2 × 250 mL), dried ($MgSO_4$), and filtered, and the solvent was evaporated, leaving macrocycle **14** as a colorless solid (5.32 g) quantitatively, mp 167−169 °C; ^{1}H NMR (300 MHz, $CDCl_3$): δ 1.20 (s, 18H; C(CH_3)$_3$), 1.62 (br m, 2H; δ-H), 1.75 (br s, 4H; NH_2), 2.43 (s, 6H; CH_3), 2.87 (s, 4H; ϵ-H), 3.04 (t, ^3J = 7.7 Hz, 4H; γ-H), 4.00 (s, 4H; α-H), 4.62 (s, 4H; β-H), 7.19 (d, ^4J = 2.3 Hz, 2H; 5-H), 7.30 (d, ^3J = 8.1 Hz, 4H; c-H), 7.30 (d, ^4J = 2.3 Hz, 4H; 3-H), 7.69 ppm (d, ^3J = 8.1 Hz, 4H; b-H); ^{13}C NMR (75 MHz, $CDCl_3$): δ 21.9 (CH_3), 25.9 (δ-H), 31.3 (C(CH_3)$_3$), 35.1 (C(CH$_3$)$_3$), 37.2 (ϵ-H), 44.9 (γ-H), 46.2 (α-H), 49.6 (β-H), 124.9 (5-C), 125.5 (3-C), 127.4 (b-C), 127.7 (1-C), 130.2 (c-C), 137.6 (a-C), 140.6 (6-C), 143.7 (d-C), 147.6 (2-C), 153.3 ppm (4-C); HRMS (ESI): calcd for $C_{43}H_{59}N_4O_4S_4$ [M + H^+], 823.34137; found 823.34258.

Macrocycle 15. Thionyl chloride (0.02 mL, 0.27 mmol) was added to a solution of macrocycle **12** (0.101 g, 0.12 mmol) and pyridine (0.03 mL, 0.36 mmol) in dichloromethane (5 mL) at 0 °C. After stirring for 21 h at room temperature, the reaction mixture was diluted with dichloromethane (25 mL) and washed with water (3 × 20 mL). The combined organic phases were dried ($MgSO_4$), filtered, and evaporated to dryness. Column chromatography (silica, 1:1 dichloromethane/heptane) afforded macrocycle **15** (0.085 g) as a colorless solid in 81% yield, mp 129−130 °C; ^{1}H NMR (300 MHz, $CDCl_3$): δ 1.22 (s, 18H; C(CH_3)$_3$), 1.66 (br m, 2H; δ-H), 2.43 (s, 6H; CH_3), 2.97 (s, 4H; ϵ-H), 3.06 (t, ^3J = 8.0 Hz, 4H; γ-H), 4.62 (s, 4H; β-H), 4.88 (s, 4H; α-H), 7.30 (d, ^3J = 8.6 Hz, 4H; c-H), 7.32 (d, ^4J = 2.4 Hz, 2H; 5-H), 7.40 (d, ^4J = 2.4 Hz, 2H; 3-H), 7.69 ppm (d, ^3J = 8.6 Hz, 4H; b-H); ^{13}C NMR (125 MHz, $CDCl_3$): δ 21.8 (CH_3), 25.5 (δ-C), 31.2 (C(CH_3)$_3$), 35.1 (C(CH$_3$)$_3$), 37.2 (ϵ-C), 44.9 (γ-C), 46.1 (α-C), 49.5 (β-C), 126.6 (5-C), 127.4 (b-C), 127.7 (3-C), 128.9 (1-C), 130.3 (c-C), 137.6 (a-C), 141.1 (6-C), 142.2 (2-C), 143.8 (d-C), 153.5 ppm (4-C); HRMS (ESI): calcd for $C_{43}H_{54}Cl_2N_2NaO_4S_4$ [M + Na^+], 883.22357; found 883.22799.

Macrocycle 16. Diiodine (0.612 g, 2.41 mmol), imidazole (0.067 g, 0.96 mmol), and finally a solution of macrocycle **12** (0.398 g, 0.48 mmol) in dichloromethane (20 mL) were sequentially added to a stirred solution of triphenylphosphine (0.634 g, 2.41 mmol) in dichloromethane (25 mL) at 0 °C, allowing 10 min periods between each addition. After 2 h stirring the reaction was quenched by addition of water (40 mL) and dichloromethane (50 mL). The organic layer was washed with sodium hydrogencarbonate (5% aqueous solution, 2 × 45 mL) and sodium hydrogensulfite (0.1% aqueous solution, 2 × 45 mL), dried ($MgSO_4$), and filtered, and the solvent was evaporated. Macrocycle **16** crystallized from 1:10 dichloromethane/ethanol (22 mL) as colorless aggregates (0.405 g) in 80% yield, mp 202−204 °C; ^{1}H NMR (300 MHz, $CDCl_3$): δ 1.20 (s, 18H; C(CH_3)$_3$), 1.65 (br m, 2H; δ-H), 2.43 (s, 6H; CH_3), 3.05 (t, ^3J = 7.7 Hz, 4H; γ-H), 3.06 (s, 4H; ϵ-H), 4.62 (s, 4H; β-H), 4.76 (s, 4H; α-H), 7.23 (d, ^4J = 2.3 Hz, 2H; 5-H), 7.30 (d, ^3J = 8.1 Hz, 4H; c-H), 7.37 (d, ^4J = 2.3 Hz, 2H; 3-H), 7.69 ppm (d, ^3J = 8.1 Hz, 4H; b-H); ^{13}C NMR (75 MHz, $CDCl_3$): δ 6.5 (α-C), 21.9 (CH_3), 25.4 (δ-C), 31.2 (C(CH_3)$_3$), 35.0 (C(CH$_3$)$_3$), 36.0 (ϵ-H), 44.7 (γ-C), 49.3 (β-H), 126.0 (5-C), 127.4 (b-C), 127.6 (3-C), 128.0 (1-C), 130.3 (c-C), 137.6 (a-C), 141.3 (6-C), 143.8 (2-C), 144.0 (d-C), 153.5 ppm (4-C); elemental analysis calcd (%) for $C_{43}H_{54}I_2N_2O_4S_4$ (1044.98): C 49.43, H 5.21, N 2.68; found: C 49.34, H 5.19, N 2.68. HRMS (ESI): calcd for $C_{43}H_{54}I_2N_2NaO_4S_4$ [M + Na^+], 1067.09480; found 1067.09825.

Macrotricycle 17. Separate solutions of macrocycle **10** (2.50 g, 3.04 mmol) and macrocycle **14** (2.51 g, 3.04 mmol) each in dichloromethane (100 mL) were added simultaneously over 15 h to a suspension of 3 Å molecular sieves in dichloromethane (175 mL) at 30 °C. After stirring for a week, the solvent was evaporated and the residue was taken up in THF (250 mL) and methanol (250 mL). The brown suspension was chilled to 0 °C and treated with sodium borohydride (0.115 g, 3.04 mmol). After 3 h stirring, sodium hydrogen-carbonate was added (5% aqueous solution, 250 mL). The mixture was then diluted with dichloromethane (400 mL) and water (200 mL). The aqueous layer was extracted with dichloromethane (2 × 250 mL). The organic layer was washed with water (2 × 300 mL), dried ($MgSO_4$), filtered and the solvent evaporated. The resulting tan solid was crystallized from 2:5 dichloromethane/ethanol (70 mL). Macrotricycle **17** was obtained as colorless crystals (3.502 g) in 71% yield. Crystals of [**17**·2H]$(CF_3CO_2)_2$ suitable for X-ray diffraction were obtained by layering with cyclohexane a solution of macrotricycle **17** (0.020 g, 0.0124 mol) and trifluoroacetic acid (0.002 mL, 0.0273 mmol) in dichloromethane (3 mL). **17**, mp 238−239 °C; ^{1}H NMR (500 MHz, $CDCl_3$): δ 1.20 (s, 36H; C(CH_3)$_3$), 1.55 (br m, 6H; δ-H and NH), 2.44 (s, 12H; CH_3), 2.97 (s, 8H; ϵ-H), 3.00 (br t, 8H; γ-H) 4.00 (s, 8H; α-H), 4.62 (s, 8H; β-H), 7.23 (d, ^4J = 2.0 Hz, 4H; 5-H), 7.32 (d, ^3J = 8.5 Hz, 8H; c-H), 7.42 (d, ^4J = 2.0 Hz, 4H; 3-H), 7.72 ppm (d, ^3J = 8.5 Hz, 8H; b-H); ^{13}C NMR (75 MHz, $CDCl_3$): δ 21.9 (CH_3), 25.8 (δ-C), 31.4 (C(CH_3)$_3$), 35.1 (C(CH$_3$)$_3$), 37.3 (ϵ-C), 45.0 (γ-C), 49.9 (β-C), 53.8 (α-C), 124.9 (5-C), 125.9 (3-C), 127.4 (b-C), 128.5 (1-C), 130.3 (c-C), 137.5 (a-C), 140.5 (6-C), 143.8 (d-C), 144.6 (2-C), 153.1 ppm (4-C); MS (MALDI-TOF): *m*/*z* (%): 1612.4 [M^+], 1456.7 [M^+ − Ts]; elemental analysis calcd (%) for $C_{86}H_{110}N_6O_8S_8$ (1612.38): C 64.06, H 6.88, N 5.21; found: C 64.16, H 7.01, N 5.01.

Macropentacycle 5 and Macrononacycle 18. A solution of macrotricycle **17** (2.315 g, 1.43 mmol) and macrocycle **16** (1.50 g, 1.43 mmol) in 1:1 toluene/acetonitrile (86 mL) was added, over 24 h, to a suspension of cesium carbonate (4.685 g, 14.35 mmol) in 1:1 toluene/acetonitrile (430 mL) at 50 °C. After 5 days of stirring, the solvents were evaporated and the residue was taken up in dichloromethane (300 mL). The organic layer was washed

with water (3 × 150 mL), dried ($MgSO_4$), filtered, and concentrated to 40 mL. The resulting solution was treated with a solution of trifluoromethanesulfonic acid (0.500 g, 3.3 mmol) in dichloromethane (10 mL) and refluxed for 36 h. The residue obtained after evaporation of the solvent was dissolved in the minimum amount of dichloromethane (10 mL), and the resulting solution layered with 1:1 dichloromethane/ethylacetate (10 mL) and ethyl acetate (40 mL). Slow evaporation (48 h) afforded colorless crystals (in fact a mixture of [**5**·H](OTf)[22] and **18**) which were collected and rinsed with ethyl acetate (3 × 30 mL). [**5**·H](OTf) and **18** were separated by column chromatography on silica eluting with 20% heptane/dichloromethane, 10% methanol/dichloromethane gradient. Monoprotonated macropentacycle [**5**·H](OTf) was obtained as a colorless solid (1.95 g) in 53% yield and macrononacycle **18** was obtained as a colorless solid (0.512 g) in 7% yield.

Free base macropentacycle **5** was obtained as follows: a solution of sodium methoxide (10 mL, 0.172 M, 1.7 mmol) in methanol was added to a solution of [**5**·H](OTf) (0.217 g, 0.085 mmol) in methanol (20 mL). After 24 h stirring the solvent was evaporated. The residue was taken up in dichloromethane (20 mL) and the organic layer washed with water (2 × 20 mL), dried ($MgSO_4$), filtered, and evaporated to dryness, leaving macropentacycle **5** as a colorless solid (0.200 g) in 98% yield. Crystals suitable for X-ray diffraction were obtained by slow evaporation of a 1:1 acetonitrile/dichloromethane solution.

5, mp 240−244 °C. ^{1}H NMR (500 MHz, $C_2D_2Cl_4$, 380 K): δ 1.28 (s, 54H; *t*-Bu-*H*), 1.65 (br m, 6H; δ-H), 2.41 (s, 18H; e-H), 2.92 (s, 12H; ϵ-H), 3.14 (br t, 12H; γ-H), 4.19 (s, 12H; α-H), 4.67 (s, 12H; β-H), 7.24 (d, ^3J = 7.8 Hz, 12H; c-H), 7.47 (s, 6H; 5-H), 7.67 (d, ^3J = 7.8 Hz, 12H; b-H), 7.76 ppm (s, 6H; 3-H); ^{13}C NMR (151 MHz, $C_2D_2Cl_4$, 350 K): δ 21.2 (*C*H_3), 25.6 (δ-C), 30.8 (C(*C*H_3)$_3$), 34.4 (*C*(CH$_3$)$_3$), 38.8 (ϵ-C), 45.5 (γ-C), 50.4 (β-C), 58.1 (α-C), 126.2 (5-C), 126.6 (3-C), 127.1 (b-C), 129.6 (c-C), 130.6 (1-C), 137.4 (a-C), 140.4 (6-C), 143.0 (2-C), 143.2 (d-C), 152.2 (4-C); ^{1}H NMR (500 MHz, CD_2Cl_2, 200 K): δ −0.47 (br s, 2H; δ'_{AD}-H and δ'_{CF}-H), 0.54 (br s, 1H; δ_{CF}-H), 0.65 (br s, 1H; δ_{AD}-H), 0.92 (s, 9H; *t*-Bu$_C$-H), 1.07 (s, 9H; *t*-Bu$_A$-H), 1.19 (s, 9H; *t*-Bu$_E$-H), 1.21 (s, 9H; *t*-Bu$_B$-H), 1.26 (s, 9H; *t*-Bu$_D$-H), 1.30 (s, 9H; *t*-Bu$_F$-H), 1.43 (br s, 1H; δ'_{BE}-H), 1.54 (br t, 1H; ϵ'_D-H), 1.96 (br s, 6H; e_F and e_D), 2.00 (br m, 2H; ϵ_D-H and ϵ_E-H), 2.10 (br s, 2H; δ_{BE}-H and γ'_C-H), 2.22 (d, ^2J = 12.5 Hz, 1H; γ'_A-H), 2.35 (s, 3H; e_E-H), 2.38 (s, 3H; e_A-H), 2.39 (s, 3H; e_C-H), 2.42 (s, 4H; ϵ_F-H and e_B-H), 2.54 (br m, 2H; γ'_B-H and ϵ'_F-H), 2.63−2.76 (br m, 3H; ϵ'_B-H, ϵ_A-H and γ'_E-H), 2.78 (d, ^2J = 12.0 Hz, 1H; α'_D-H), 2.87 (br t, 1H; γ_D-H), 2.91 (d, ^2J = 11.0 Hz, 2H; α'_E-H and γ_F-H), 2.95−3.10 (br m, 4H; γ_C-H, γ_A-H, ϵ'_C-H, ϵ_B-H), 3.12 (d, ^2J = 11 Hz, 1H; β'_A-H), 3.18 (br d, ^2J = 8 Hz, 1H; β'_C-H), 3.27 (d, ^2J = 10.5 Hz, 1H; α'_F-H), 3.39 (br t, 1H; γ_B-H), 3.45−3.63 (br m, 3H; γ'_F-H, γ'_D-H and ϵ_C-H), 3.67 (d, ^2J = 16.5 Hz, 1H; α'_C-H), 3.70 (br d, ^2J = 12.0 Hz, 1H; ϵ'_A-H), 3.77 (d, ^2J = 12.0 Hz, 1H; α_D-H), 3.86 (br s, 1H; γ_E-H), 3.88 (br s, 2H; α_B-H and α'_B-H), 4.02 (d, ^2J = 16.3 Hz, 2H; α'_A-H and ϵ'_E-H), 4.12 (d, ^2J = 18.3 Hz, 1H; β'_E-H), 4.39 (d, ^2J = 15.0 Hz, 1H; β'_B-H), 4.60 (d, ^2J = 17.0 Hz, 1H; β'_D-H), 4.64−4.77 (br m, 4H; β'_F-H, α_E-H, α_F-H and β_D-H), 4.82 (d, ^2J = 15.0 Hz, 1H; β_B-H), 4.86 (d, ^2J = 18.3 Hz, 1H; β_E-H), 5.16−5.25 (br m, 2H; β_A-H and β_F-H), 5.27 (br d, ^2J = 8 Hz, 1H; β_C-H), 5.38 (d, ^2J = 16.3 Hz, 1H; α_A-H), 5.45 (d, ^2J = 16.5 Hz, 1H; α_C-H), 6.09 (d, ^3J = 7.5 Hz, 2H; c_D-H), 6.43 (br s, 2H; c_F-H), 6.80 (s, 1H; 5_C-H), 6.88 (s, 1H; 5_A-H), 7.19 (d, ^3J = 7.5 Hz, 2H; c_E-H), 7.25−7.40 (m, 12H; c_A, 5_E, c_B, 3_D, c_C, b_F and b_D), 7.44 (s, 1H; 3_E-H), 7.48 (br s, 3H; b_E-H and 3_F-H), 7.53 (d, ^3J = 7.5 Hz, 2H; b_A-H), 7.56 (d, ^3J = 8.0 Hz, 2H; b_C-H), 7.64 (s, 1H; 5_B-H, and d, ^3J = 8.5 Hz, 2H; b_B-H), 7.69 (s, 1H; 5_D-H), 7.82 (br s, 1H; 5_F-H), 7.92 (s, 1H; 3_C-H), 8.19 (s, 1H; 3_B-H), 8.22 ppm (s, 1H; 3_A-H); MS (MALDI-TOF): *m*/*z* (%): 2401.1 [M$^+$], 2245.0 [M$^+$ − Ts]; elemental analysis calcd (%) for $C_{129}H_{162}N_8O_{12}S_{12}$·0.5$CH_2Cl_2$ (2444.01): C 63.64, H 6.72, N 4.58, S 15.74; found: C 63.73, H 7.09, N 4.99, S 15.78.

18, mp 257−260 °C; ^{1}H NMR (500 MHz, $C_2D_2Cl_4$, 340 K): δ 1.24 (two s, 36H; *t*-Bu′-*H*, and 72H; *t*-Bu-*H*), 1.53 (br m, 4H; δ-H), 1.61 (br m, 4H; δ-H), 1.95 (br m, 4H; δ'-H), 2.40 (s, 12H; e′-H), 2.46 (s, 24H; e-H), 2.77 (s, 8H; ϵ'-H), 2.96 (s, 16H; γ-H), 3.06 (br q, 16H; ϵ-H), 3.28 (br t, 8H; γ'-H), 3.88 (br s, 8H; α'-H), 3.89 (dd, ^{AB}J = 13.9 Hz, $\Delta\nu_{AB}$ = 21.9 Hz, 16H; α-H), 4.57 (s, 8H; β'-H), 4.72 (dd, ^{AB}J = 17.0 Hz, $\Delta\nu_{AB}$ = 49.3 Hz, 16H; β-H), 7.16 (s, 4H; 5′-H), 7.24 (br s, 8H; 5-H), 7.28 (d, ^3J = 8.2 Hz, 8H; c′-H), 7.35 (d, ^3J = 8.2 Hz, 16H; c-H), 7.66 (s, 4H; 3′-H), 7.67 (d, ^3J = 8.1 Hz, 8H; b′-H), 7.72 (d, ^3J = 8.1 Hz, 16H; b-H), 7.77 ppm (s, 8H; 3-H); ^{13}C NMR (151 MHz, $C_2D_2Cl_4$, 350 K): δ 21.2 (*C*H_3′), 21.3 (*C*H_3), 24.8 (δ-C), 26.0 (δ'-C), 31.0 (C(*C*H_3)$_3$′), 31.0 (C(*C*H_3)$_3$), 34.5 (*C*(CH$_3$)$_3$′ and *C*(CH$_3$)$_3$), 37.0 (ϵ'-C), 37.2 (ϵ-C), 44.0 (γ-C), 44.7 (γ'-C), 48.6 (β-C), 49.7 (β'-C), 55.4 (α'-C), 57.1 (α-C), 124.1 (5′-C), 124.4 (5-C), 125.8 (3 and 3′-C), 126.9 (b and b′-C), 128.4 (1-C), 128.5 (1′-C), 129.7 (c′-C), 129.8 (c-C), 137.3 (a′-C), 137.7 (a-C), 139.3 (6′-C), 139.8 (6-C), 143.2, 143.3 (2×), 143.6 (2, 2′, d, d′-C), 152.3 (4′-C), 152.6 (4-C); MS (TOF-ESI): *m*/*z* (%): 4802.9 [M$^+$]; elemental analysis calcd (%) for $C_{258}H_{324}N_{16}O_{24}S_{24}$ (4803.09): C 64.52, H 6.80, N 4.67, S 16.02; found: C 64.55, H 6.93, N 4.72, S 16.21.

Acknowledgment. We thank Dr. Jean-Michel Barbe and Ms. Marie-José Penouilh (ICMUB) for the EI and ESI mass spectra and Ms. Evelyne Pousson (ICMUB) for the elemental analyses. The referees are acknowledged for helpful comments.

Supporting Information Available: ORTEP views of **5**, **10**, and **18**, VT ^{1}H NMR spectra of **18**, full range ^{1}H NMR spectra of **5** in various solvents and/or at VT, low-temperature COSY and ROESY ^{1}H and ^{1}H/^{13}C HSQC NMR spectra of **5**, ^{1}H and ^{13}C NMR spectra of compounds **7**−**17**, and high-temperature ^{13}C NMR spectra of **5** and **18**. This material is available free of charge via the Internet at http://pubs.acs.org.

JO701984Z